NASA TECHNICAL NOTE

NASA TN D-4710

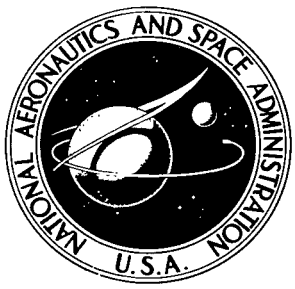

INVESTIGATION OF A COMPARTMENTED-GAS-BAG LANDING SYSTEM HAVING MULTIPLE-IMPACT CAPABILITIES

by John R. McGehee

Langley Research Center

Langley Station, Hampton, Va.

NATIONAL AERONAUTICS AND SPACE ADMINISTRATION • WASHINGTON, D. C. • AUGUST 1968

INVESTIGATION OF A COMPARTMENTED-GAS-BAG LANDING SYSTEM HAVING MULTIPLE-IMPACT CAPABILITIES

By John R. McGehee

Langley Research Center
Langley Station, Hampton, Va.

NATIONAL AERONAUTICS AND SPACE ADMINISTRATION

For sale by the Clearinghouse for Federal Scientific and Technical Information
Springfield, Virginia 22151 – CFSTI price $3.00

INVESTIGATION OF A COMPARTMENTED-GAS-BAG LANDING SYSTEM HAVING MULTIPLE-IMPACT CAPABILITIES

By John R. McGehee
Langley Research Center

SUMMARY

The principles of a proposed gas-bag landing system having omnidirectional, multiple-impact, and kinetic-energy-dissipating capabilities have been investigated experimentally and analytically. The omnidirectional capability of the proposed system may be obtained by surrounding the payload with a radially compartmented, spherical, gas bag. The multiple-impact capability may be achieved by retaining all gas within the bag during impacts. Kinetic energy may be dissipated by gas flow through orifices in the compartment walls and the resulting phase lag between the internal gas-flow cycle and the impact-rebound cycle.

The principles of the proposed landing system were investigated experimentally to determine the kinetic-energy-dissipating capability of the system. A simplified test vehicle, using unidirectional gas bags, was tested with both sharp-edged and fabric-covered orifices between the compartments. A supplementary experimental investigation was conducted to determine the discharge parameters associated with various fabrics. In addition, equations were derived for computing time histories of acceleration, velocity, stroke, and compartment pressures to extend the usefulness of the investigation by permitting variation of the landing environment and test vehicle parameters.

The results of the experimental investigation show a kinetic-energy-dissipation capability for the initial impact as great as 93 percent of the vehicle touchdown kinetic energy. Tests performed with aircraft-fabric-covered orifices yielded a slightly greater (approximately 5 percent) kinetic-energy-dissipation capability than was obtained with the sharp-edged orifices. The analytical investigation resulted in a computational procedure which provides fair agreement between computed and experimentally determined accelerations, pressures, and kinetic-energy dissipation for the ranges of velocity and bag initial pressures investigated.

INTRODUCTION

Programs have been proposed which envision the use of instrumented, soft-landing capsules for early planetary exploration. The task of designing landing systems for

survivable landings of instrumented capsules is complicated by inadequate data on the atmospheres and surface structures of the planets (refs. 1 and 2). Because of these uncertainties it would appear that a landing system having omnidirectional and multiple-impact capabilities would enhance the probability of achieving a successful landing. A variety of gas-compression systems have been proposed and investigated for use as energy-absorbing landing systems (refs. 3 to 11). The military services have used air bags for the aerial delivery of cargo and the Mercury spacecraft were equipped with an air-bag system for shock attenuation during landings. Spherical gas bags have been investigated, both analytically and experimentally, to provide a landing system having omnidirectional capabilities. (See refs. 3, 4, and 5.) The systems previously investigated, however, did not have a multiple-impact capability since they were designed to release gas from the bags either through orifices during the compression cycle or by bag rupture at the end of the compression cycle.

The purpose of the present investigation was to study the principles of a proposed gas-bag landing system having omnidirectional, multiple-impact, and kinetic-energy-dissipating capabilities. In the proposed landing system a spherical gas bag would surround the capsule for omnidirectional capability and gas would be retained within the bag during impacts for multiple-impact capability. Kinetic energy would be dissipated by having the gas bag compartmented so that gas would be forced through orifices between compartments. During the initial impact, gas compression would occur in those compartments in contact with the landing surface and the gas forced through orifices in the compartment walls into the uncompressed or storage compartments. The force resulting from the pressure generated in the compressed compartments would stop the vehicle, although some of the touchdown kinetic energy would, of course, remain in the pressurized gas of the compartments in contact with the landing surface and this pressure could initiate rebound. Assuming that all of the available stroke would be used (maximum gas exhaustion), rebound would still occur due to the return flow of gas from the storage compartments. Thus, at the instant of rebound initiation (for strokes less than the maximum available stroke), gas would still be flowing from the compressed compartments into the storage compartments. Hence, a phase lag exists between the internal gas-flow cycle and the impact-rebound cycle so that some of the kinetic energy which would be stored as potential energy in the form of increased pressure in the storage compartments during impact would not be available during rebound. The orifices, which control the flow, may be thought of as valves which partially block or throttle flow during vehicle rebound and prevent reconversion of the potential energy into vehicle kinetic energy. During rebound the vehicle would lose contact with the surface and the internal gas flow cycle would reverse, so that gas would flow from the storage compartments back into the formerly compressed compartments, returning the bag to its spherical shape. In

subsequent impacts this cycle would be repeated until the other natural energy dissipating mechanisms (such as friction) eventually bring the vehicle to rest.

The principles of the proposed landing system were investigated experimentally to determine the kinetic-energy-dissipating capability of the system. A simplified test vehicle, utilizing the principle of the proposed system, was tested with both sharp-edged and fabric-covered orifices between the compartments. A supplementary experimental investigation was necessary to determine the discharge parameters of the fabric-covered orifices and is included as appendix A. In addition, equations were derived for computing time histories of acceleration, velocity, stroke, and compartment pressures to extend the usefulness of the investigation to the design of landing systems requiring different sizes, masses, impact velocities, and gravity conditions. Data obtained from the analytical investigation were compared with the experimental data.

SYMBOLS

The units used for the physical quantities in this paper are given both in the International System of Units (SI) and in the U.S. Customary Units. Factors relating the two systems are given in reference 12 and those used in the present investigation are presented in appendix B.

A	area, meters^2 (feet^2)
C	orifice discharge coefficient
d	diameter, meters (feet)
F	force, newtons (pounds force)
g	acceleration due to gravity, 9.81 meters per second^2 (32.2 feet per second^2)
K	flow direction indicator
m_{air}	mass of air, kilograms (slugs)
m_{conf}	mass of configuration decelerated, kilograms (slugs)
p	pressure, kilonewtons per meter^2 (pounds per inch^2)
p_h	head pressure, meters of H_2O (feet of H_2O)

Q	mass flow of air, grams per second (slugs/second)
r	radius of the cylindrical gas bags, meters (feet)
t	time from instant of contact, seconds
V	volume, meters^3 (feet^3)
y	air-bag stroke, meters (feet)
$\dot{y}$	velocity, meters per second (feet per second)
$\ddot{y}$	acceleration, meters per second^2 (feet per second^2)
λ	geometric porosity of fabrics (ratio of area of open space to total area)
ρ	mass density of air (at standard conditions 1.22557 kilograms per meter^3 (0.002378 slug per foot^3))

Subscripts:

a	atmospheric
e	exhausted
f	footprint (area of gas bag in contact with landing surface)
i	initial
o	orifice
t	time after contact
v	vehicle
w	water

I refers to collapsible volume

II, III, IV refer to storage volumes in the order of association with collapsible volume

APPARATUS AND PROCEDURE

Experimental Investigation

It was noted in the introduction that in order to obtain omnidirectional and multiple-impact landing capabilities the payload could be surrounded by a spherical-shaped, gas-bag, landing system. One such landing system, a spherical-shaped gas bag having 20 equal volume compartments with interconnecting orifices, is illustrated in the sketch of figure 1. An impact on the sphere at a vertex common to five compartments (fig. 1) would result in compression of the five compartments with subsequent gas flow into three additional sets of five compartments. For the experimental investigation a simplified test vehicle was designed to simulate conditions that would exist for the impact of the spherical gas bag on a vertex common to five compartments. A sketch of the test vehicle and orifice details are shown in figure 2. Pertinent parameters of this vehicle are presented in table I. In order to determine the influence of orifice design on the performance of the vehicle, both sharp-edged and fabric-covered orifices (fig. 2) were investigated in landings of the test vehicle.

Test vehicle.- The test vehicle size was selected for convenience in the conduct of the experiments. The vehicle was cylindrical and had an overall height of 0.43 m (1.4 ft), a maximum diameter of 0.30 m (1 ft), and a decelerated mass of 11.09 kg (0.76 slug). The decelerated mass is defined as the total mass of the vehicle minus the mass of the base plate and one-half the sum of the mass of the collapsible bags. The volume of the collapsible gas bags and the volumes of each of the three storage compartments were each one-fourth the total volume within the test vehicle.

The collapsible gas bags were designed to decelerate the vehicle from a velocity of 4.24 m/s (13.9 fps) with an initial air-bag pressure of 0 kN/m^2 (0 psig) without exceeding the stroke of the air bags. The total gas-bag volume was equally divided into eight cylindrical air bags. Each bag was made of a single layer of 0.025-cm (0.010 in.) balloon cloth (rubber-impregnated cotton fabric) and each had a diameter of 8.00 cm (3.00 in.) and a collapsible length or stroke of 0.15 m (0.5 ft). Multiple bags were used to obtain better stability of the test vehicle relative to that obtainable with a single bag. The upper body was a cylindrical aluminum can and had two plywood partitions with aluminum orifice plates. (See fig. 2.) For the sharp-edged orifices the orifice areas between the four volumes were each 0.0008 m^2 (0.0086 ft^2). The orifices between compartments were staggered to avoid air mass transfer which would result if the jet of air from one orifice impinged upon another orifice.

The fabric-covered orifices (fig. 2) had coverings of aircraft fabric (cotton). In order to facilitate the comparison of kinetic-energy dissipation for the vehicle tests with sharp-edged orifices and fabric-covered orifices, the orifice areas for the fabric-covered orifices were increased by the ratio of the discharge parameter of the sharp-edged orifice to that of the selected fabric. Discharge parameters for fabric-covered orifices are discussed in appendix A. This modification was made to obtain approximately the same stroking of the air bags with fabric-covered orifices as was achieved in landings of the vehicle with sharp-edged orifices.

Instrumentation.- A photograph of the test vehicle and the instrumentation used in the landing experiments is shown as figure 3. The instrumentation consisted of a single component strain-gage type accelerometer, four strain-gage type pressure transducers, 20 kHz (20 kcps) carrier amplifier, an air-pressure control, and a recording oscillograph. The accelerometer has a natural frequency of 465 Hz (465 cps), was damped to 89 percent of critical damping, and was capable of measuring ±50 g units. The accelerometer, as used in these tests, had a calibration factor of 2.90 g units/cm (7.36 g units/in.). The accelerometer was rigidly mounted to the lead mass (as shown in fig. 2) to measure accelerations along the longitudinal axis of the vehicle. The pressure transducers are capable of measuring 345 kN/m (50 psi) with a natural frequency of approximately 10 kHz (10 kcps) and, for these tests, had calibration factors of approximately 19 $kN/m^2/cm$ (7 psi/in.). A pressure transducer was mounted to record the gage pressure in each of the four volumes. It should be noted, however, that the pressure in the collapsible gas-bag volume was measured in only one of the eight bags and as shown in figure 2 it was necessary to mount the gage internally; thus, a vent tube was required from the back of the gage to the atmosphere. The response of the recording equipment for acceleration recording was flat to 60 Hz (60 cps) and for pressure recording was flat to 1000 Hz (1000 cps).

Test methods.- All tests were made by a free-fall method. Tests were made for vertical contact velocities of 4.24 m/s (13.9 fps) and 6.00 m/s (19.7 ft/sec). All landings were made on concrete for 0^o (symmetrical) contact attitude.

The experimentally obtained acceleration time histories were used to determine the kinetic energy dissipated in percent of the kinetic energy of the vehicle at contact with the landing surface. The acceleration time histories were integrated from a reference line of 1 g unit. The velocity thus obtained was used in conjunction with the touchdown velocity to determine the kinetic energy dissipated.

Analytical Investigation

Equations were derived, utilizing the equations of motion and the force-stroke characteristics of the gas bags, to permit the computation of time histories of acceleration and

pressure for landings from a vertical flight path at a 0^{o} (symmetrical) contact attitude. In the derivation of the equations of this analysis, it was assumed that the gas bags were inextensible and flexible and the only force-causing deceleration was the gas-pressure force. The discharge parameter for the sharp-edged orifices was 0.6. The discharge parameters for the fabric-covered orifices were determined from the results of the discharge parameter investigation. (See appendix A.) Equations were developed for both isothermal and adiabatic flow. The computations were made by using a numerical integration procedure which employs the transformation $d^2y/dt^2 = \Delta\dot{y}/\Delta t$. The incremental time Δt was chosen sufficiently small so that the pressure and density at the beginning of any time interval could be taken as the average pressure and density during the time interval. The equations derived for these computations are presented in appendix C.

Time histories of acceleration, velocity, stroke, and pressure were computed for selected values of initial pressure and contact velocity used in the experimental program. The computations were performed through the time required to obtain maximum rebound velocity. The maximum rebound velocity, constant vehicle mass being assumed, was used to compute the kinetic energy dissipated in percent of vehicle kinetic energy at initial contact.

RESULTS AND DISCUSSION

Experimental Investigation

The results of the test vehicle investigation are presented in figures 4 to 7. Figure 4 shows typical oscillograph records of vehicle acceleration and compartment pressures for both sharp-edged and fabric-covered orifices. The shaded area under each acceleration curve was integrated to obtain the value of velocity (sum of the initial contact velocity and the maximum rebound velocity) to be employed in computing the kinetic energy dissipated during an impact.

Typical time histories of acceleration and pressure for landings made with the test vehicle are shown in figure 5 for the range of initial pressures investigated. The distortion near the peaks of the acceleration curves and the pressure curves for V_I are believed to result from unsymmetrical compression of the gas bags and the associated pitching of the upper body. As a result of the mass associated with the instrument cable (fig. 3) and since the tests were conducted by having the vehicle fall freely to the landing surface, perfectly symmetrical compression of the cylindrical air bags did not occur. Consequently, the pressure curve for V_I would not necessarily represent the pressure associated with acceleration, since the pressure for V_I was measured in only one of the eight cylindrical bags. Hence, direct correlation between time histories of acceleration and V_I pressure was not obtained in all cases. Orifice-throttling characteristics may

be illustrated by noting the difference in the peak pressures between V_I and V_{II}. For example, the data in figure 5(a) show a peak pressure for V_{II} that is 25 percent less than that for V_I. Increases in initial pressure resulted in a decrease in the difference between the peak pressures in V_I and V_{II}. (See fig. 5(b).)

The results of the discharge parameter investigation (appendix A) indicated that aircraft fabric had a maximum discharge parameter of 0.06 which is approximately one-tenth that of the sharp-edged orifices. In order to compare kinetic-energy losses between tests of the vehicle with the fabric-covered orifices and the sharp-edged orifices, similar impact parameters were required. Therefore, the area of the fabric-covered orifice was increased by a factor of 10 relative to the area of the sharp-edged orifice in order to obtain the same bag stroke for the impact velocity and initial bag pressure used in the tests with the sharp-edged orifice. The similarity of the data shown in figures 5(a) and 5(c) for the sharp-edged and fabric-covered orifices, respectively, indicates the validity of this procedure.

The V_I pressure data shown in figure 5(d) illustrate the effect of an unsymmetrical impact on the measured V_I pressure. The initial impact occurred on the collapsible bag containing the pressure pickup used for measuring V_I pressures. As a result the measured pressure is considerably higher than the pressure causing deceleration. The dashed line in this figure represents computed V_I pressures based on measured acceleration values and an assumed symmetrical impact. By using the computed V_I pressure in figure 5(d), it can be seen from figures 5(c) and 5(d) that increases in initial bag pressure also resulted in a decrease in the differences between the peak pressures in V_I and V_{II}.

Analytical Investigation

Experimental and computed time histories of acceleration and pressure are compared in figure 6 for landings made with sharp-edged and fabric-covered orifices. Computations made by assuming both adiabatic and isothermal flow are compared with experimental data obtained from the sharp-edged orifice model at an initial gage pressure of 0 kN/m^2 (0 psig) in figure 6(a). The computed values of peak acceleration agree fairly well with the magnitude of the peak experimental acceleration, but are displaced in time. As previously stated, the computations were made by assuming perfectly symmetrical impact and rebound but the experimental data, because of the free-fall test method, were not obtained for perfectly symmetrical impacts. The disagreement between the time of peak acceleration for the computed and experimental values may possibly be attributed to an unsymmetrical experimental impact which could result in a delay in the time of maximum force and, consequently, acceleration.

The pressure in V_I was measured in only one of the eight collapsible bags. An unsymmetrical impact would result in a pressure reading which would not represent the actual pressure in V_I. Therefore, agreement between experimental and computed V_I pressures would not be expected, because perfectly symmetrical experimental impacts were not achieved. Experimental and computed pressures for V_{II}, V_{III}, and V_{IV} show fair agreement.

The differences between computed time histories of acceleration and pressure with assumed adiabatic flow and those with assumed isothermal flow are believed to be within the accuracy to which experimental accelerations and pressures could be read. Hence, only computations assuming isothermal flow were made for comparison with the experimental data in figures 6(b) and 6(c). The computational procedure resulted in fair agreement between experimental and computed values of accelerations and pressures for the test ranges of velocity and bag initial pressure.

Kinetic-Energy-Dissipation Capability

The kinetic energy dissipated, expressed in percent of touchdown kinetic energy, is shown in figure 7 as a function of initial bag pressure. Experimental and computed data are presented for landings of the test vehicle with sharp-edged orifices made at velocities of 4.24 m/s (13.9 fps) and 6.00 m/s (19.7 fps). Experimental data are also presented for the test vehicle with aircraft-fabric-covered orifices landing at a velocity of 4.24 m/s (13.9 fps).

Experimental data obtained from tests of the vehicle with sharp-edged orifices for a velocity of 4.24 m/s (13.9 fps) and an initial bag pressure of 0 kN/m^2 (0 psig) indicated that approximately 88 percent of the touchdown kinetic energy was dissipated. At the same values of velocity and initial bag pressure, data from the vehicle with fabric-covered orifices indicated that approximately 93 percent of the touchdown kinetic energy was dissipated. Landings of the vehicle, with both types of orifices, at initial bag pressures greater than atmospheric and a contact velocity of 4.24 m/s (13.9 fps) indicated a decrease in kinetic-energy dissipation with increases in initial bag pressures. If flow losses are assumed to vary with the amount of flow involved, it would appear that this type of landing system would dissipate more kinetic energy for those tests in which the greater proportion of the initial volume of air was forced from the collapsible bags. In order to check the foregoing premise the vehicle with sharp-edged orifices was impacted at a velocity of 6.00 m/s (19.7 fps) for initial bag pressures of approximately 12.4 kN/m^2 (1.8 psig) and 22.1 kN/m^2 (3.2 psig). Comparing the data in figure 7 for these tests with those conducted at the same initial bag pressure but at a velocity of 4.24 m/s (13.9 fps) shows that the increased impact velocity, which results in increased stroking of the collapsible bags

since the mass is constant, produces approximately a 10-percent increase in kinetic-energy dissipation. The kinetic energy dissipated by the flow through the aircraft-fabric-covered orifices appeared to be approximately 5 percent greater than that dissipated by flow through the sharp-edged orifices. This increase in energy dissipation may possibly be attributed to increased losses resulting from additional frictional effects associated with the flow through the fabric. These losses also influence phase lag between the gas-flow cycle and the impact-rebound cycle.

The computed data for the vehicle with sharp-edged orifices are shown by the symbols with ticks in figure 7 for velocities of 4.24 m/s (13.9 fps) and 6.00 m/s (19.7 fps). The data computed for a velocity of 4.24 m/s (13.9 fps) are within 5 percent of the experimental data throughout the range of initial bag pressures investigated. The data computed (one data point) for the higher velocity are in agreement with the experimental data. Therefore, within the accuracy of the experimental investigation, it would appear that the computational procedure is adequate for predicting kinetic-energy dissipation.

CONCLUDING REMARKS

The results of the experimental investigation of a compartmented-gas-bag landing system with multiple-impact capability show a kinetic-energy-dissipation capability as great as 93 percent of the touchdown kinetic energy. Flow through aircraft-fabric-covered (cotton) orifices resulted in a slightly greater (approximately 5 percent) kinetic-energy-dissipation capability than was obtained from flow through sharp-edged orifices. The analytical investigation yielded a computational procedure which resulted in fair agreement between experimental and computed values of accelerations and pressures for the test ranges of velocity and bag initial pressure. Within the accuracy of the experimental investigation, the derived computational procedure appears to predict adequately kinetic-energy dissipation for the test ranges of velocity and initial bag pressure.

Langley Research Center,
National Aeronautics and Space Administration,
Langley Station, Hampton, Va., April 26, 1968,
124-08-04-14-23.

APPENDIX A

INVESTIGATION OF DISCHARGE PARAMETERS FOR VARIOUS FABRICS

The apparatus used in the discharge-parameter (product of discharge coefficient and geometric porosity) investigation is shown in the photograph of figure 8. The apparatus consisted of a settling chamber and a number of pressure chamber units which were attached in line with the settling chamber. An air pressure line having a maximum pressure of 621 kN/m^2 (90 psig) was connected to the settling chamber through a throttling valve. Fabric specimens and a control orifice were mounted between the flanges of the pressure chamber units. The control orifice was used to determine the mass flow of air during a test. Static and total-head pressure pickups were installed in the settling chamber and in each of the pressure chambers. These pressure pickups were connected to a water-filled manometer for obtaining pressure measurements.

A typical test run is described to illustrate the operation of the apparatus. Fabric specimens of 0.15-m (0.5 ft) diameter were mounted between the flanges of the pressure chamber units. A control orifice was mounted between the flanges of the last pressure units at the exhaust end. The throttling valve was opened to obtain the desired pressure in the settling chamber. After the flow was established a photograph of the manometer board was taken. A typical photograph of the manometer board taken during one of the experiments is shown in figure 9. The pressure drop across each of the installed specimens is shown.

Discharge parameters were determined for cotton, nylon, and glass fabrics as a function of the pressure differential across the fabrics. Various weaves and fabric thicknesses of the glass fabric were investigated. Control orifices encompassing a range of diameters from 0.254 cm (0.100 in.) to 2.357 cm (0.928 in.) were employed to obtain a range of pressure differentials from approximately 0.02 kN/m^2 (0.003 psi) to 3.00 kN/m^2 (0.400 psi). Restrictions imposed upon the airflow by the throttling valve and the pressure line limited the range of pressure differentials that could be obtained when the larger control orifices were used. Therefore, in order to obtain higher pressures in the settling chamber and, consequently, greater pressure drops across the fabric specimens when the larger control orifices were used, it was necessary to reduce the area of the fabric specimens. This was accomplished by installing backing plates with holes, having a smaller cross-sectional area than that of the 10-cm-diameter (4 in.) pipe, downstream of each of the fabric specimens.

Flow losses were determined from the measured pressure drops across the various fabrics and orifices as a function of the air mass flow. The mass flow for each of the

tests was computed from the pressure drop across the control orifice employing a discharge coefficient of 0.61 for a sharp-edged circular orifice. In each test, several fabrics were installed and the mass flow through all of these fabrics was computed by employing the measured pressure loss across the control orifice in the following equation:

$$Q = 0.61\rho A_o\dot{y} = 0.7476A_o\left(2g\ \Delta p_h\rho_w/\rho\right)^{1/2} \tag{A1}$$

where

A_o orifice area, m^2 (ft^2)

ρ_w density of water, kg/m^3 ($slugs/ft^3$)

ρ density of air flowing through orifice, kg/m^3 ($slugs/ft^3$)

Δp_h pressure drop across control orifice, m of H_2O (ft of H_2O)

The discharge parameters for each of the fabric specimens were then computed from the following equation:

$$C\lambda = \frac{Q}{\rho A_o\left(2g\ \Delta p_h\rho_w/\rho\right)^{1/2}} \tag{A2}$$

where Q was determined from equation (A1) and Δp_h was the measured pressure drop across the specimens.

Photographs of the water-filled manometer for typical discharge parameter tests are shown in figure 10 for various mass flows. Static and total-head pressures are shown and within the reading accuracy there was no discernible difference between the static and total-head pressures for the range of mass flows.

The discharge parameters (defined herein as the product of the discharge coefficient C and the geometric porosity λ) for a sharp-edged orifice and various fabrics are presented in figure 11 as a function of the pressure differential across the orifice or fabric. The experimentally obtained discharge parameters (discharge coefficients since $\lambda = 1.0$) for the 0.254-cm-diameter (0.100 in.) orifices were approximately 0.59. This value is approximately 3 percent below the 0.61 coefficient normally accepted for the boundary proportions of the equipment used in this test $\left(\frac{\text{Orifice diameter}}{\text{Pipe diameter}} = \frac{0.254\text{ cm}}{10.16\text{ cm}}\left(\frac{0.100\text{ in.}}{4.000\text{ in.}}\right) = 0.025\right)$.

The increase in the discharge parameter with increasing pressure differential for the various fabrics is believed to result primarily from an increase in the geometric porosity of the fabric as it stretches. This hypothesis appears to be substantiated by the

data obtained for the two glass fabrics. The type VIII glass fabric appears to reach a constant value of the discharge parameter of 0.033 at a pressure differential of approximately 3.0 kN/m^2 (0.44 psi), thus indicating that the glass fabric has become taut and reached a fixed value of porosity and, consequently, a fixed value of the discharge parameter. The type III glass fabric appears to follow the same trend, but because it is a lighter material it reaches a constant value of the discharge parameter of 0.045 at a pressure differential of approximately 0.4 kN/m^2 (0.06 psi). (For a description of the glass fabrics, see ref. 13.) The type VIII fabric has the appearance of being less porous than the type III fabric and the data also indicate that this is the case since the type VIII fabric has a lower maximum value of discharge parameter. Within the range of pressure differentials investigated, the discharge parameters for the aircraft fabric (cotton) and the parachute fabric (nylon) did not reach a constant maximum value. The data for these fabrics were extrapolated, on the basis of the results obtained with the glass fabrics, to obtain a constant maximum value of the discharge parameter. This maximum value of discharge parameter obtained from the extrapolation for the parachute fabric was 0.1 at a pressure differential of approximately 10 kN/m^2 (1.45 psi) and for the aircraft fabric it was 0.06 at a pressure differential of approximately 10 kN/m^2 (1.45 psi).

The results of the discharge-parameter investigation for the fabrics tested indicate that there is a range of pressure differentials within which the discharge parameter increases with increasing pressure differential. The results also indicate that the discharge parameters approach a maximum value as the pressure differential increases.

APPENDIX B

CONVERSION OF U.S. CUSTOMARY UNITS TO SI UNITS

The International System of Units (SI) was adopted by the Eleventh General Conference on Weights and Measures, Paris, October 1960, in Resolution No. 12 (ref. 12). Conversion factors for the units used herein are given in the following table:

Physical quantity	U.S. Customary Unit	Conversion factor (*)	SI Unit
Length	ft	0.3048	meters (m)
Force	lbf	4.448	newtons (N)
Density	slugs/ft^3	515.38	kg/m^3
Pressure	psi = lbf/in^2	6.8948	kN/m^2
Mass	slugs	14.594	kg
Energy	ft-lbf	1.3558	joule, (J)
Mass flow	slugs/sec	14.595	kg/s
Velocity	ft/sec	0.3048	m/s
Acceleration	ft/sec^2	0.3048	m/s^2
Frequency	cps	1.0000	hertz (Hz)

*Multiply value given in U.S. Customary Unit by conversion factor to obtain equivalent value in SI unit.

Prefixes to indicate multiple of units are as follows:

Prefix	Multiple
kilo (k)	10^3
centi (c)	10^{-2}
milli (m)	10^{-3}

APPENDIX C

EQUATIONS FOR COMPUTING TIME HISTORIES OF ACCELERATION AND PRESSURE

Isothermal Flow

The decelerating force at any time after contact with the landing surface is equal to the product of the footprint area of the compressible bags and the gage pressure in the bags

$$F_t = A_f\left(p_{I,t}\right)_{gage}$$

where the footprint area of the bags is

$$A_f = 8\pi r^2$$

The gage pressure in the compressible bags at any time t after contact may be determined from the pressure-volume relation and the mass-flow equations. When isothermal compression and expansion are assumed

$$\left(p_{I,t}\right)_{gage} = \frac{p_{I,i}V_{I,i}}{V_{I,t}}\left[\frac{\left(m_{air,I}\right)_i - \left(m_{air,e,I}\right)_t}{\left(m_{air,I}\right)_i}\right] - p_a$$

where $\left(m_{air,e,I}\right)_t$ is the total mass of gas exhausted from the compressible bags into the first storage volume at time t.

The volume of air in the compressible bags at any time t after contact may be computed from the following equation:

$$V_{I,t} = V_{I,i} - A_f y_t$$

where $A_f y_t$ represents the volume change due to compression.

The mass of air in the compressible bags at contact is

$$\left(m_{air,I}\right)_i = \rho_{I,i}V_{I,i}$$

The air mass exhausted from the compressible bags $\left(m_{air,e,I}\right)_t$ at any time t is approximated by

$$\left(m_{air,e,I}\right)_t = \sum \rho C A_o \, \Delta t \sqrt{\frac{2\left|p_{I,t-1} - p_{II,t-1}\right|}{\rho}}\left(\frac{p_{I,t-1} - p_{II,t-1}}{\left|p_{I,t-1} - p_{II,t-1}\right|}\right)$$

Note that temperature effects are ignored and the velocity through the orifice is limited to sonic velocity by the following relation: For $\sqrt{\frac{2\left|p_{I,t-1} - p_{II,t-1}\right|}{\rho}} \geqq \sqrt{\frac{1.4p_a}{\rho_a}}$, use $\sqrt{\frac{1.4p_a}{\rho_a}}$.

In order to account for gas flow reversal between impact and rebound cycles, the following relations apply: When $K_I = \frac{p_{I,t-1} - p_{II,t-1}}{\left|p_{I,t-1} - p_{II,t-1}\right|} \geqq 0$, $\rho = \rho_{I,t-1}$; conversely, when $K_I < 0$, $\rho = \rho_{II,t-1}$ where $\rho_{I,t-1} = \frac{p_{I,t-1}}{p_{I,i}} \rho_{I,i}$ and $\rho_{II,t-1} = \frac{p_{II,t-1}}{p_{II,i}} \rho_{II,i}$.

The equations derived for determining the absolute pressure in storage volumes II, III, and IV at any time after contact are

$$p_{II,t} = \left[\frac{\left(m_{air,II}\right)_i + \left(m_{air,e,I}\right)_t - \left(m_{air,e,II}\right)_t}{\left(m_{air,II}\right)_i}\right] p_{II,i}$$

$$p_{III,t} = \left[\frac{\left(m_{air,III}\right)_i + \left(m_{air,e,II}\right)_t - \left(m_{air,e,III}\right)_t}{\left(m_{air,III}\right)_i}\right] p_{III,i}$$

$$p_{IV,t} = \left[\frac{\left(m_{air,IV}\right)_i + \left(m_{air,e,III}\right)_t}{\left(m_{air,IV}\right)_i}\right] p_{IV,i}$$

The mass exhausted from volume II at any time after contact is approximated by

$$\left(m_{air,e,II}\right)_t = \sum \rho C A_0 \, \Delta t \sqrt{\frac{2\left|p_{II,t-1} - p_{III,t-1}\right|}{\rho}} \left(\frac{p_{II,t-1} - p_{III,t-1}}{\left|p_{II,t-1} - p_{III,t-1}\right|}\right)$$

For $\sqrt{\frac{2\left|p_{II,t-1} - p_{III,t-1}\right|}{\rho}} \geqq \sqrt{\frac{1.4p_a}{\rho_a}}$, use $\sqrt{\frac{1.4p_a}{\rho_a}}$.

In order to account for gas flow reversal between impact and rebound cycles, the following relations apply: When $K_{II} = \frac{p_{II,t-1} - p_{III,t-1}}{\left|p_{II,t-1} - p_{III,t-1}\right|} \geqq 0$, $\rho = \rho_{II,t-1}$; conversely, when $K_{II} < 0$, $\rho = \rho_{III,t-1}$. The mass exhausted from volume III at any time after contact is approximated by

$$\left(m_{air,e,III}\right)_t = \sum \rho C A_0 \, \Delta t \sqrt{\frac{2\left|p_{III,t-1} - p_{IV,t-1}\right|}{\rho}} \left(\frac{p_{III,t-1} - p_{IV,t-1}}{\left|p_{III,t-1} - p_{IV,t-1}\right|}\right)$$

APPENDIX C

For $\sqrt{\frac{2\left|p_{III,t-1} - p_{IV,t-1}\right|}{\rho}} \geqq \sqrt{\frac{1.4p_a}{\rho_a}}$, use $\sqrt{\frac{1.4p_a}{\rho_a}}$.

In order to account for gas flow reversal between impact and rebound cycles, the following relations apply: When $K_{III} = \frac{p_{III,t-1} - p_{IV,t-1}}{\left|p_{III,t-1} - p_{IV,t-1}\right|} \geqq 0$, $\rho = \rho_{III,t-1}$; conversely, when $K_{III} < 0$, $\rho = \rho_{IV,t-1}$.

The deceleration at any time t may now be computed as follows:

$$\ddot{y}_t = \frac{F_t}{m_{conf}} - g$$

The velocity at the end of the time interval or, synonymously, the velocity at the beginning of the next time interval may now be computed as follows:

$$\dot{y}_t = \dot{y}_{t-1} - \ddot{y}_t \, \Delta t$$

Adiabatic Flow

The pressure-volume relation and the mass-flow equations for assumed adiabatic compression and expansion of the air are presented.

The gage pressure in the collapsible bags at any time t after contact is

$$\left(p_{I,t}\right)_{gage} = \frac{p_{I,i}\left(V_{I,i}\right)^{1.4}}{\left(V_{I,t}\right)^{1.4}}\left[\frac{\left(m_{air,I}\right)_i - \left(m_{air,e,I}\right)_t}{\left(m_{air,I}\right)_i}\right]^{1.4} - p_a$$

where

$$V_{I,t} = V_{I,i} - A_f y_t$$

and

$$\left(m_{air,e,I}\right)_t \approx \sum \rho C A_0 \, \Delta t \sqrt{\frac{2\left|p_{I,t-1} - p_{II,t-1}\right|}{\rho}}\left(\frac{p_{I,t-1} - p_{II,t-1}}{\left|p_{I,t-1} - p_{II,t-1}\right|}\right)$$

Note that the velocity through the orifices is limited to sonic velocity by the following relation: For $\sqrt{\frac{2\left|p_{I,t-1} - p_{II,t-1}\right|}{\rho}} \geqq \sqrt{\frac{1.4p_{I,t-1}}{\rho_{I,t-1}}}$, use $\sqrt{\frac{1.4p_{I,t-1}}{\rho_{I,t-1}}}$.

APPENDIX C

In order to account for gas flow reversal between impact and rebound cycles, the following relations apply: When $K_I = \left(\frac{p_{I,t-1} - p_{II,t-1}}{|p_{I,t-1} - p_{II,t-1}|}\right) \geq 0$, $\rho = \rho_{I,t-1}$; conversely, when $K_I < 0$, $\rho = \rho_{II,t-1}$.

The absolute pressure in storage volumes II, III, and IV at any time after contact may be obtained from the following equations:

$$p_{II,t} = \left[\frac{(m_{air,II})_i + (m_{air,e,I})_t - (m_{air,e,II})_t}{(m_{air,II})_i}\right]^{1.4} p_{II,i}$$

$$p_{III,t} = \left[\frac{(m_{air,III})_i + (m_{air,e,II})_t - (m_{air,e,III})_t}{(m_{air,III})_i}\right]^{1.4} p_{III,i}$$

$$p_{IV,t} = \left(\frac{m_{IV,i} + m_{IIIe,t}}{m_{IV,i}}\right)^{1.4} p_{IV,i}$$

The mass of air exhausted from volume II at any time t after contact may be approximated by

$$(m_{air,e,II})_t = \sum \rho C A_0 \, \Delta t \sqrt{\frac{2|p_{II,t-1} - p_{III,t-1}|}{\rho}} \left(\frac{p_{II,t-1} - p_{III,t-1}}{|p_{II,t-1} - p_{III,t-1}|}\right)$$

For $\sqrt{\frac{2|p_{II,t-1} - p_{III,t-1}|}{\rho}} \geq \sqrt{\frac{1.4 p_{II,t-1}}{\rho_{II,t-1}}}$, use $\sqrt{\frac{1.4 p_{II,t-1}}{\rho_{II,t-1}}}$.

In order to account for gas flow reversal between impact and rebound cycles, the following relations apply: When $K_{II} = \left(\frac{p_{II,t-1} - p_{III,t-1}}{|p_{II,t-1} - p_{III,t-1}|}\right) \geq 0$, $\rho = \rho_{II,t-1}$; conversely, when $K_{II} < 0$; $\rho = \rho_{III,t-1}$. The mass of air exhausted from volume III at any time t after contact may be approximated by

$$(m_{air,e,III})_t = \sum \rho C A_0 \, \Delta t \sqrt{\frac{2|p_{III,t-1} - p_{IV,t-1}|}{\rho}} \left(\frac{p_{III,t-1} - p_{IV,t-1}}{|p_{III,t-1} - p_{IV,t-1}|}\right)$$

For $\sqrt{\frac{2|p_{III,t-1} - p_{IV,t-1}|}{\rho}} \geq \sqrt{\frac{1.4 p_{III,t-1}}{\rho_{III,t-1}}}$, use $\sqrt{\frac{1.4 p_{III,t-1}}{\rho_{III,t-1}}}$.

APPENDIX C

In order to account for gas flow reversal between impact and rebound cycles, the following relations apply: When $K_{III} = \left(\frac{p_{III,t-1} - p_{IV,t-1}}{|p_{III,t-1} - p_{IV,t-1}|} \right) \geqq 0$, $\rho = \rho_{III,t-1}$; conversely, when $K_{III} < 0$, $\rho = \rho_{IV,t-1}$.

REFERENCES

1. Evans, Dallas E.; Pitts, David E.; and Kraus, Gary L.: Venus and Mars Nominal Natural Environment for Advanced Manned Planetary Mission Programs. NASA SP-3016, 1965.

2. Spencer, D. F.: *Engineering Models of the Martian Atmosphere and Surface.* Tech. Mem. 33-234 (Contract No. NAS 7-100), Jet Propulsion Lab., California Inst. Technol., July 1, 1965.

3. Martin, E. Dale; and Howe, John T.: An Analysis of the Impact Motion of an Inflated Sphere Landing Vehicle. NASA TN D-314, 1960.

4. Howe, John T.; and Martin, E. Dale: Gas Dynamics of an Inflated Sphere Striking a Surface. NASA TN D-315, 1960.

5. Esgar, Jack B.; and Morgan, William C.: Analytical Study of Soft Landings on Gas-Filled Bags. NASA TR R-75, 1960.

6. Stubbs, Sandy M.; and McGehee, John R.: Investigation of the Landing Characteristics of a Reentry Vehicle Having a Canted Multiple-Air-Bag Load-Alleviation System. NASA TN D-1934, 1963.

7. Tomcsak, Stephen L.: Decelerator Bag Study. WADC TR 59-775, U.S. Air Force, June 1960.

8. Matlock, Hudson; and Thompson, J. Neils: High-Velocity Impact Cushioning. Part III – Preliminary Tests on a Nonpressurized Air Bag. Contract DA 19-129-QM-817, Struct. Mech. Res. Lab., Univ. of Texas, Oct. 15, 1957. (Available from DDC as AD No. 220 822.)

9. McGehee, John R.; and Vaughan, Victor L., Jr.: Model Investigation of the Landing Characteristics of a Reentry Spacecraft With a Vertical-Cylinder Air Bag for Load Alleviation. NASA TN D-1027, 1962.

10. McGehee, John R.; and Hathaway, Melvin E.: Landing Characteristics of a Reentry Capsule With a Torus-Shaped Air Bag for Load Alleviation. NASA TN D-628, 1960.

11. Ross, R. G., Jr.; and Layman, W. E.: The Design and Testing of an Inflated Sphere Impact Limiter. Tech Rep. No. 32-1037 (Contract No. NAS 7-100), Jet Propulsion Lab., California Inst. Technol., Dec. 15, 1966.

12. Comm. on Metric Pract.: ASTM Metric Practice Guide. NBS Handbook 102, U.S. Dep. Com., Mar. 10, 1967.

13. Anon.: Cloth, Glass, Finished, for Polyester Resin Laminates. Mil. Specif. MIL-C-9084B, Jan. 22, 1960.

TABLE I.- PERTINENT PARAMETERS OF TEST VEHICLE

Decelerated mass	11.09 kg	(0.76 slug)
Footprint area of collapsible bags	0.036 m^2	(0.393 ft^2)
Volumes:		
V_I (collapsible bags)	0.006 m^3	(0.196 ft^3)
V_{II}	0.006 m^3	(0.196 ft^3)
V_{III}	0.006 m^3	(0.196 ft^3)
V_{IV}	0.006 m^3	(0.196 ft^3)
Orifice area:		
Sharp-edged orifice tests –		
Between V_I and V_{II}	0.0008 m^2	(0.0086 ft^2)
Between V_{II} and V_{III}	0.0008 m^2	(0.0086 ft^2)
Between V_{III} and V_{IV}	0.0008 m^2	(0.0086 ft^2)
Fabric-covered orifice tests –		
Between V_I and V_{II}	0.0079 m^2	(0.0855 ft^2)
Between V_{II} and V_{III}	0.0079 m^2	(0.0855 ft^2)
Between V_{III} and V_{IV}	0.0079 m^2	(0.0855 ft^2)
Maximum stroke of collapsible bags	0.15 m	(0.50 ft)

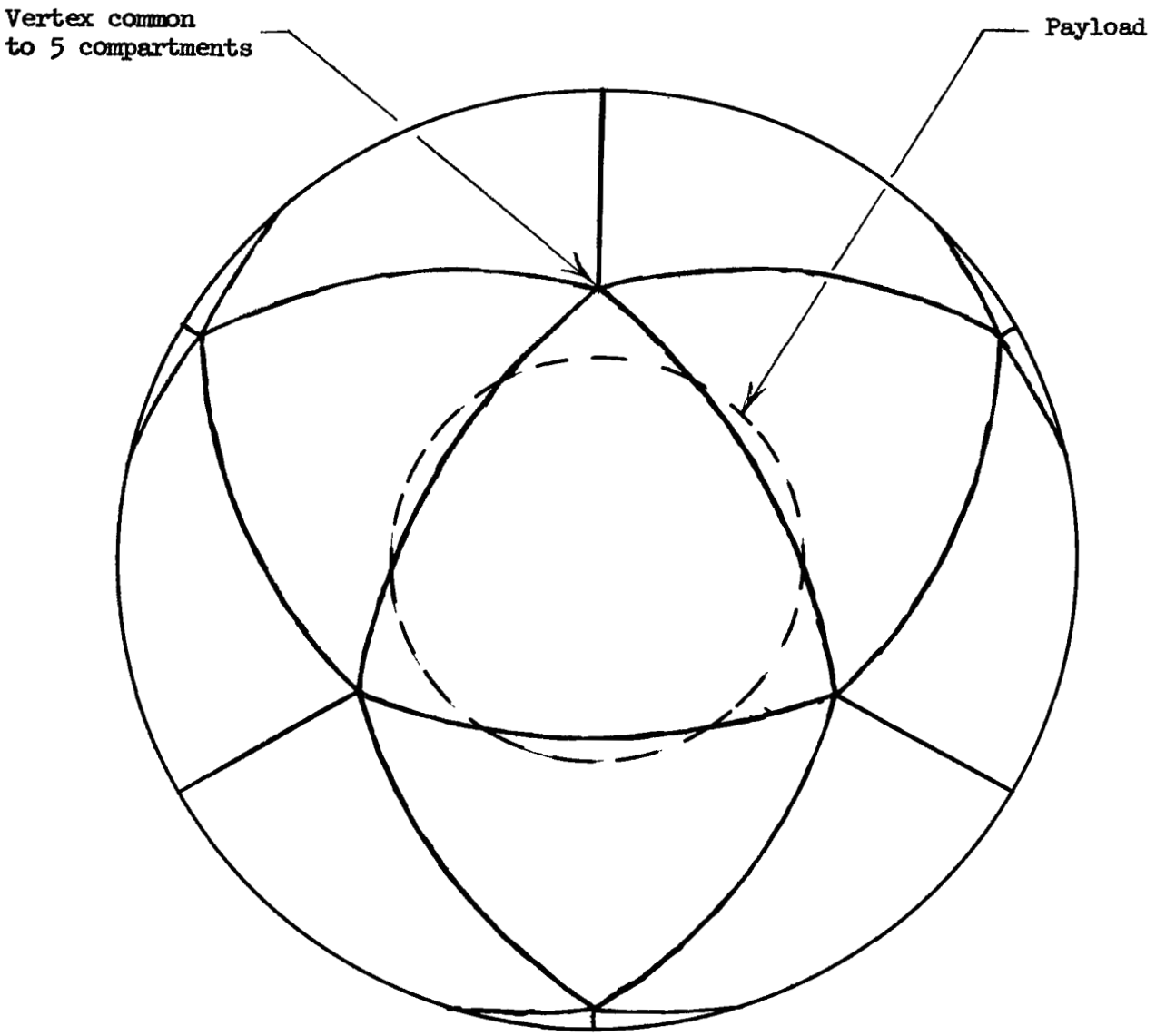

Figure 1.- Sketch of a spherical gas bag having 20 equal volume compartments.

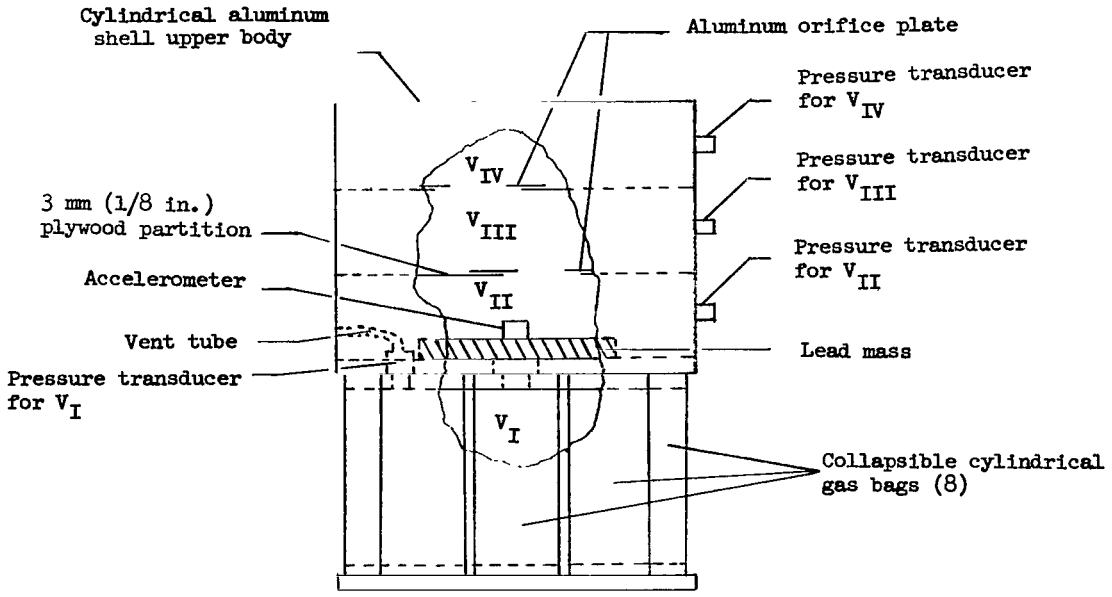

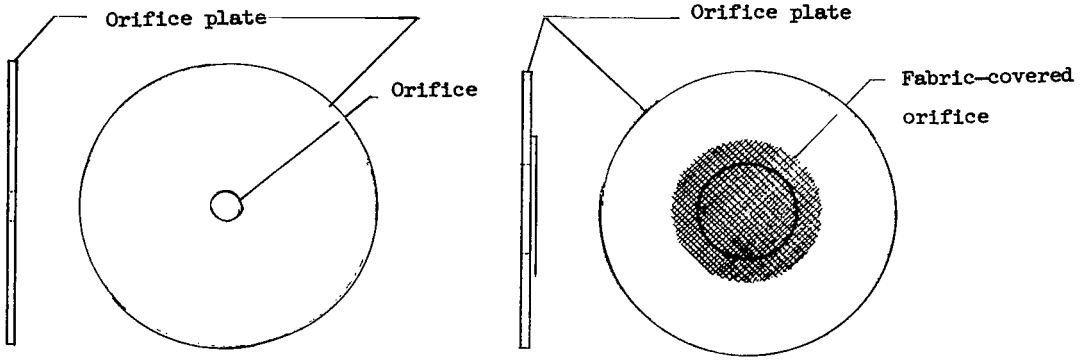

Figure 2.- Sketch of test vehicle and details of orifices.

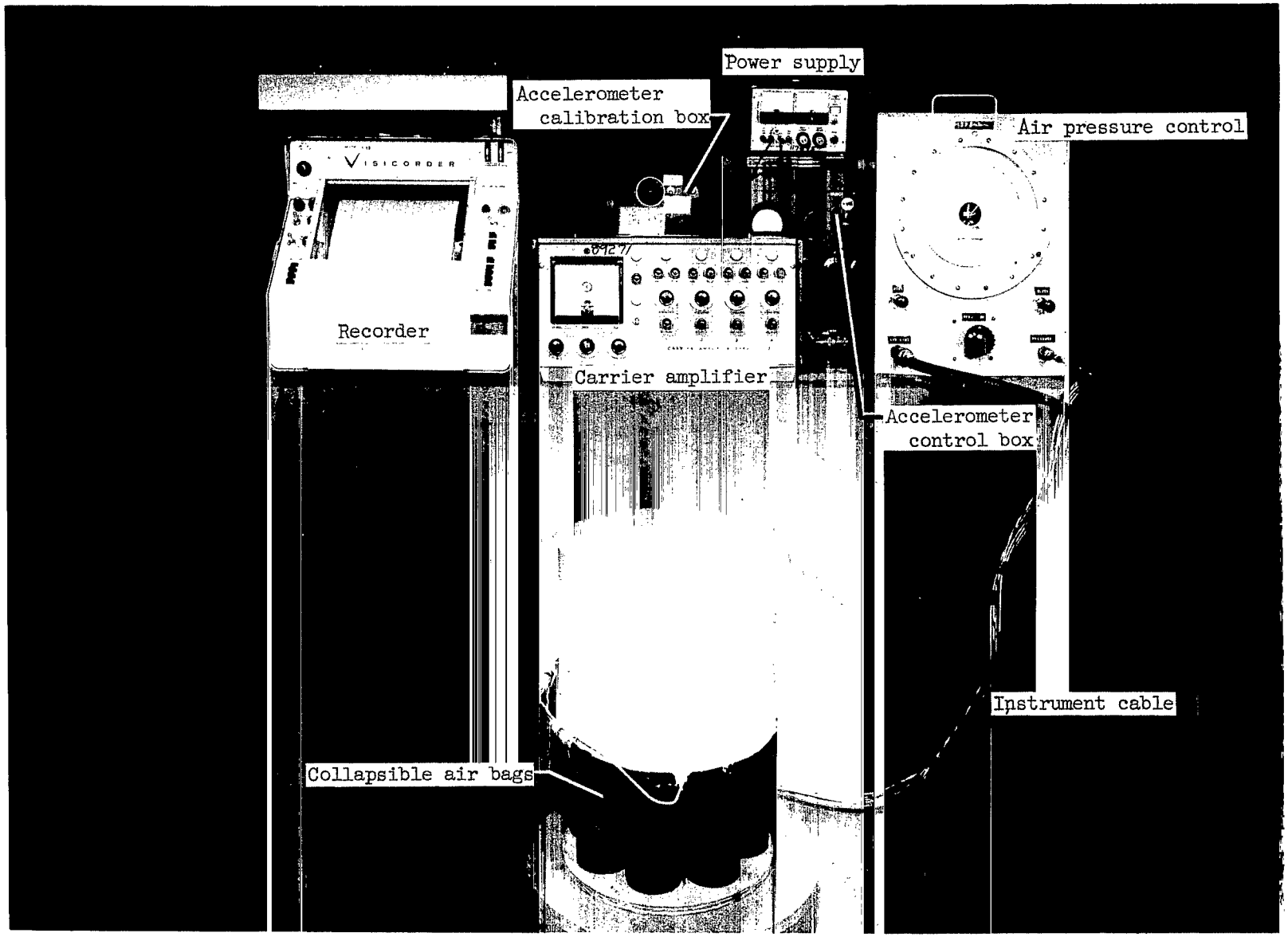

Figure 3.- Test vehicle and instrumentation.

L-66-3364.1

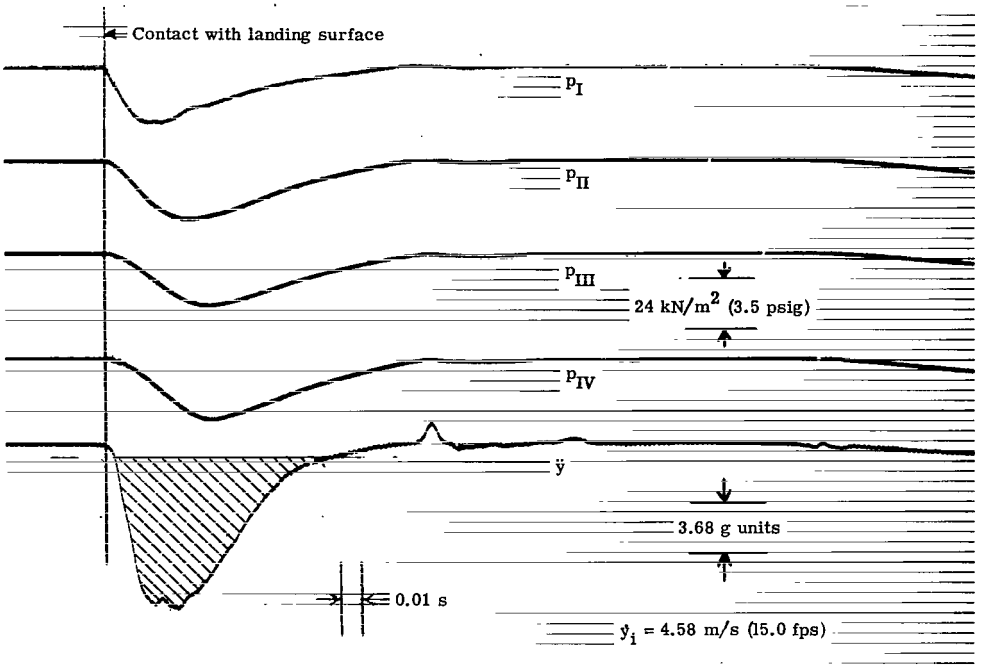

(a) Test vehicle with sharp-edged orifices; $p_{i,gage}$ = 0 kN/m^2 (0 psi).

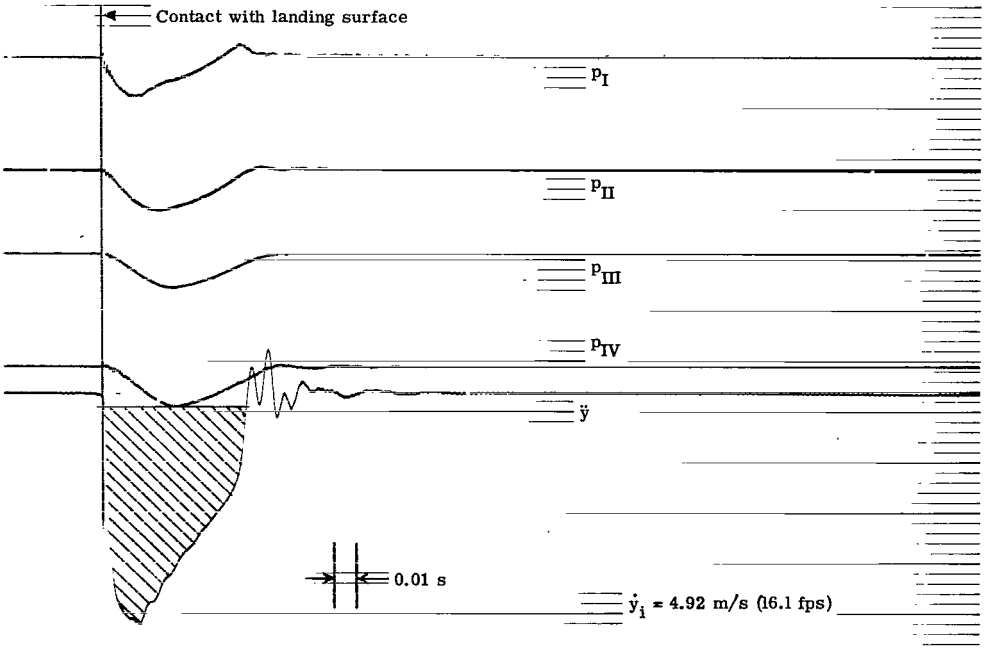

(b) Test vehicle with sharp-edged orifices; $p_{i,gage}$ = 24.0 kN/m^2 (3.5 psi).

Figure 4.- Typical oscillograph records obtained from test vehicle.

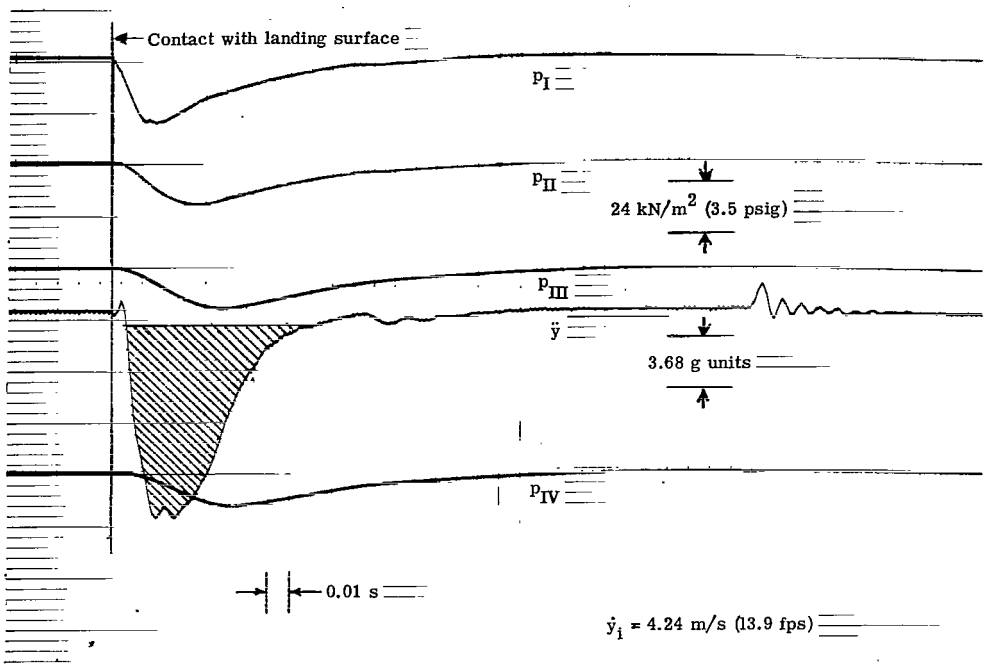

(c) Test vehicle with aircraft-fabric-covered orifices; $p_{i,gage}$ = 0 kN/m^2 (0 psi).

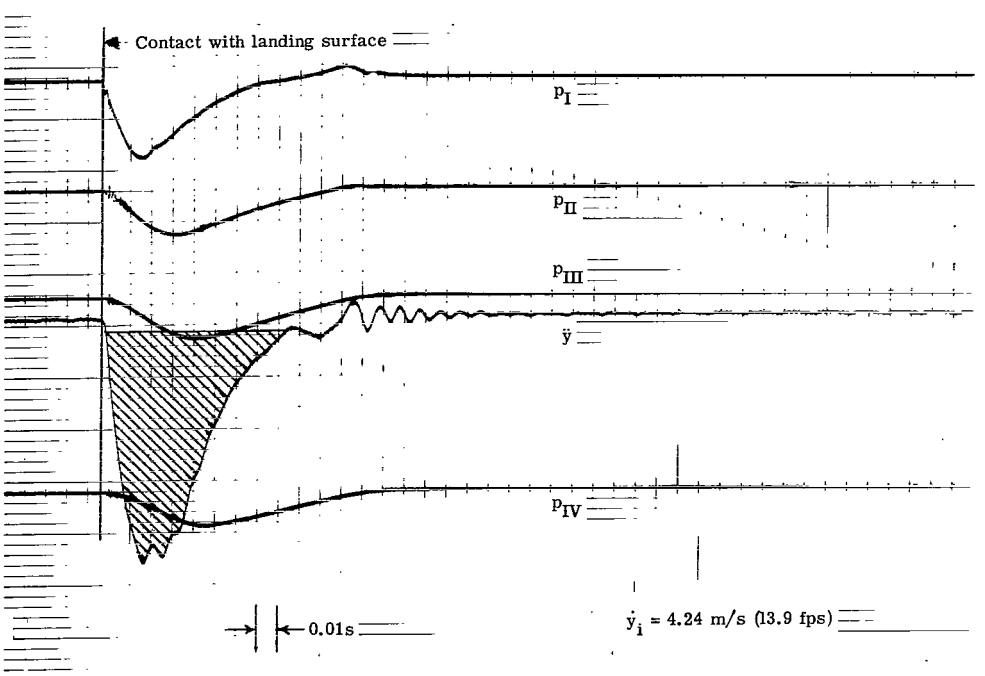

(d) Test vehicle with aircraft-fabric-covered orifices; $p_{i,gage}$ = 10.3 kN/m^2 (1.5 psi).

Figure 4.- Concluded.

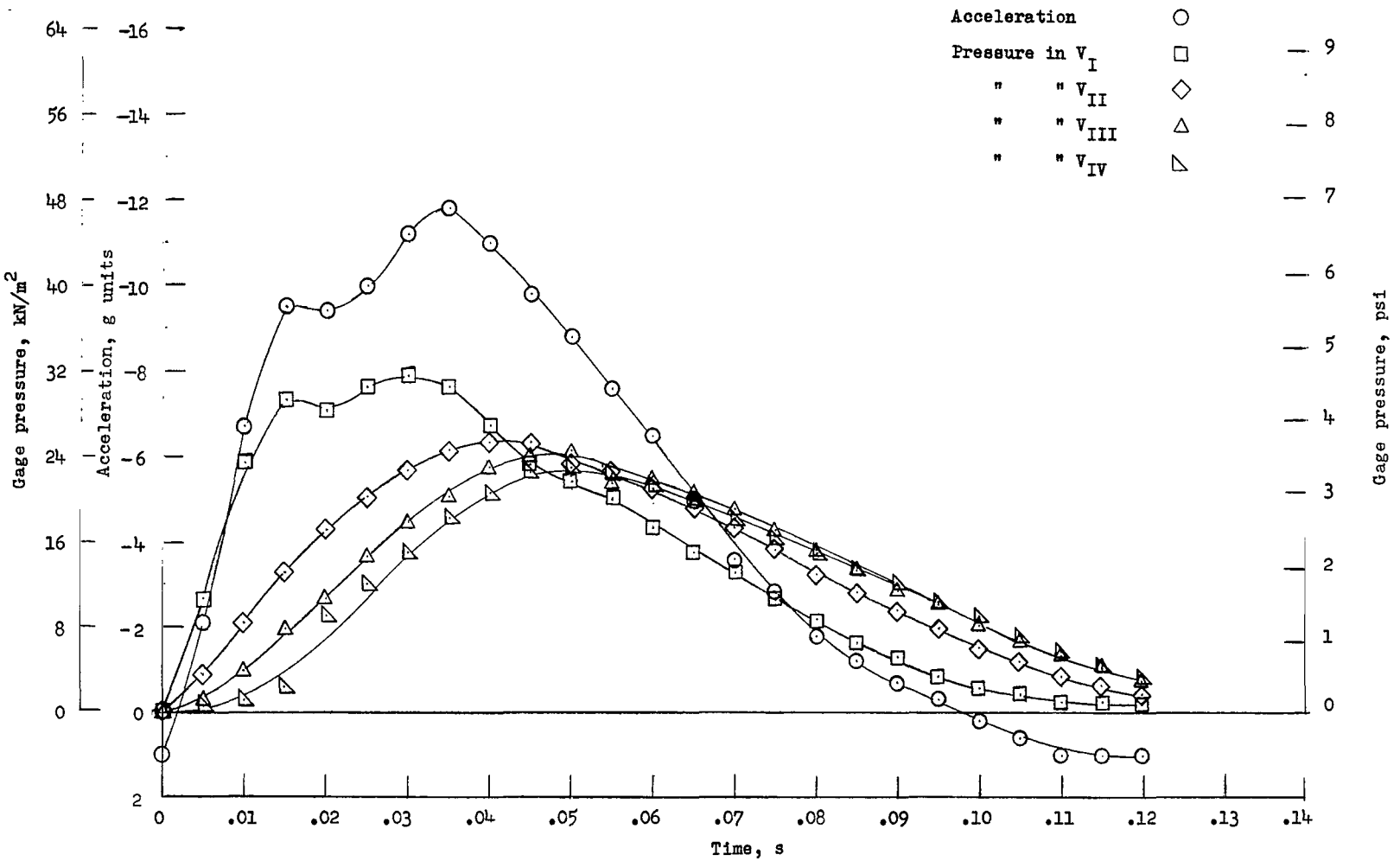

(a) Sharp-edged orifices; $p_{i,gage} = 0$ kN/m^2 (0 psi).

Figure 5.- Typical time histories of acceleration and pressure obtained from test vehicle. $\dot{y}_i = 4.24$ m/s (13.9 fps).

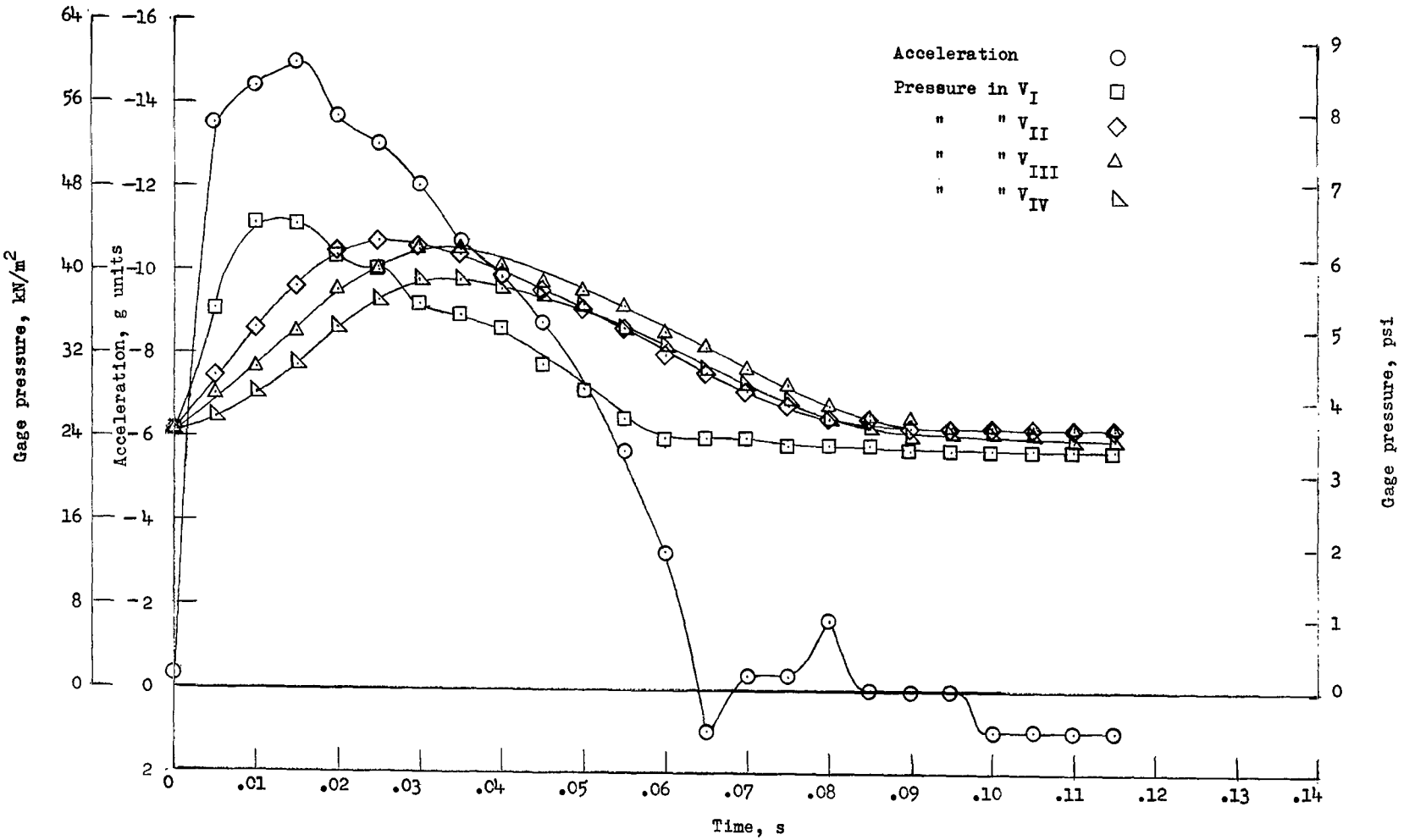

(b) Sharp-edged orifices, $p_{i,gage}$ = 24.8 kN/m2 (3.6 psi).

Figure 5.- Continued.

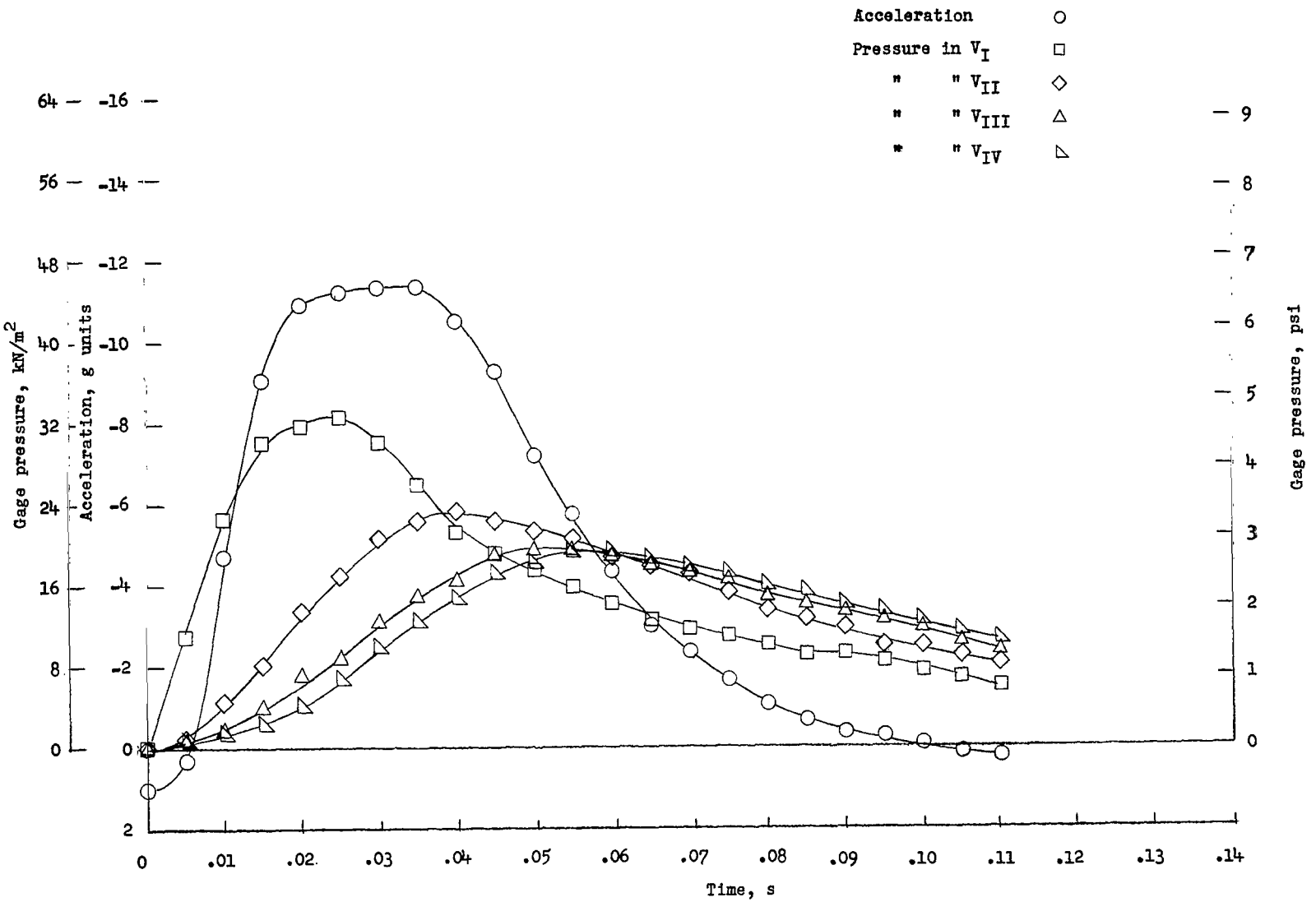

(c) Aircraft-fabric-covered orifices; $p_{i,gage}$ = 0 kN/m² (0 psi).

Figure 5.- Continued.

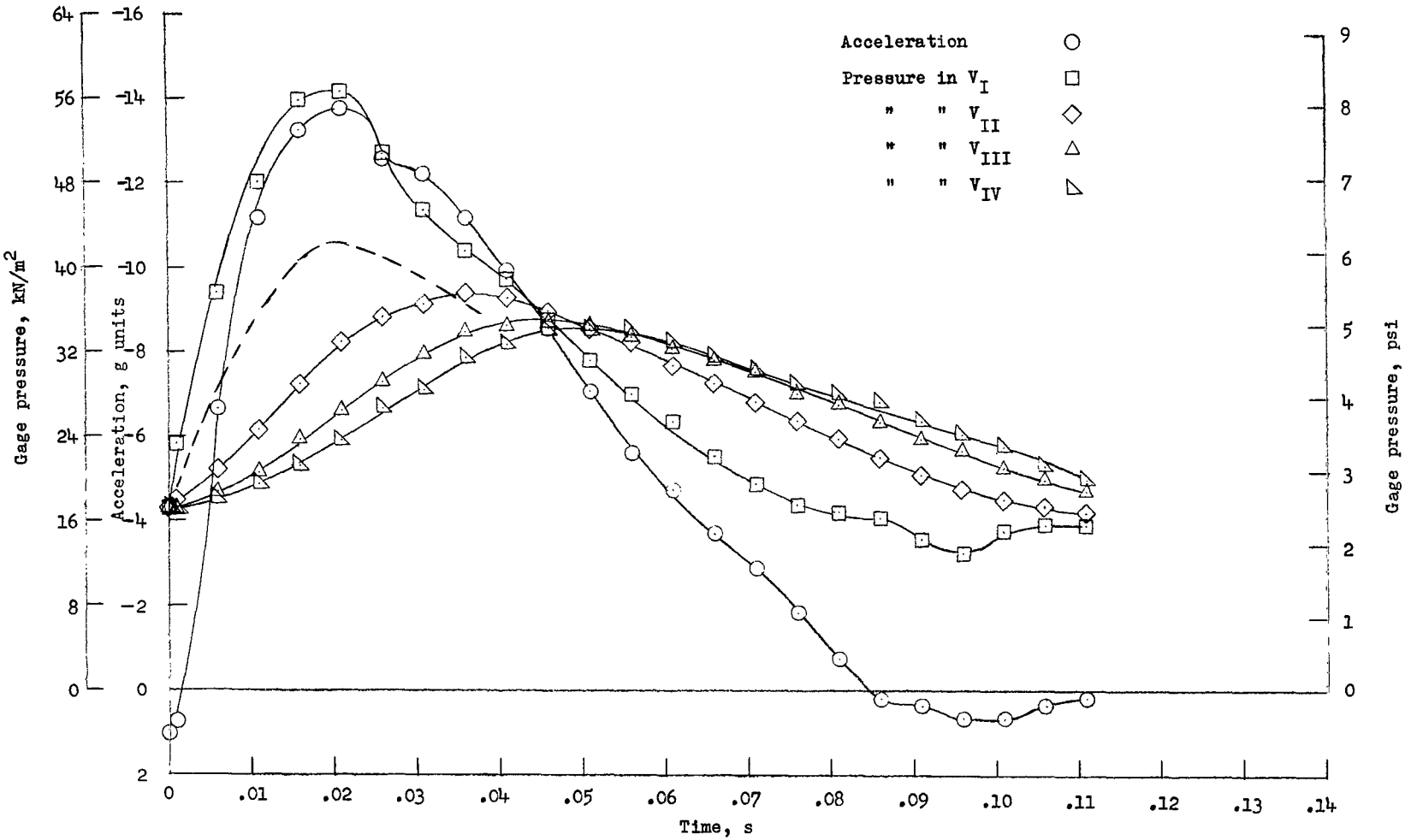

(d) Aircraft-fabric-covered orifices; $p_{i,gage}$ = 17.2 kN/m^2 (2.5 psi).

Figure 5.- Concluded.

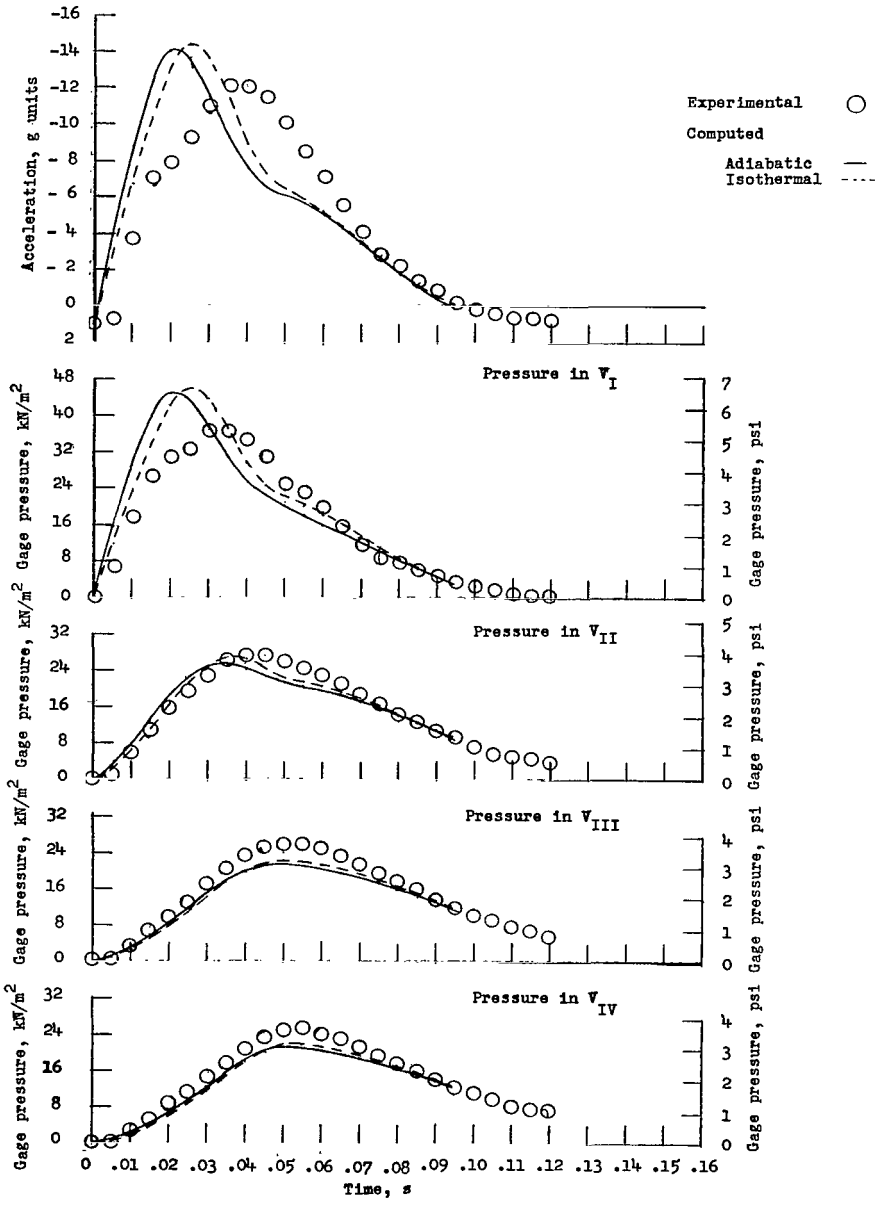

(a) Test vehicle with sharp-edged orifices; p_i = 0 kN/m^2 (0 psi).

Figure 6.- Comparison of typical time histories of experimental and computed acceleration and pressures. $\dot{y}_i$ = 4.24 m/s (13.9 fps).

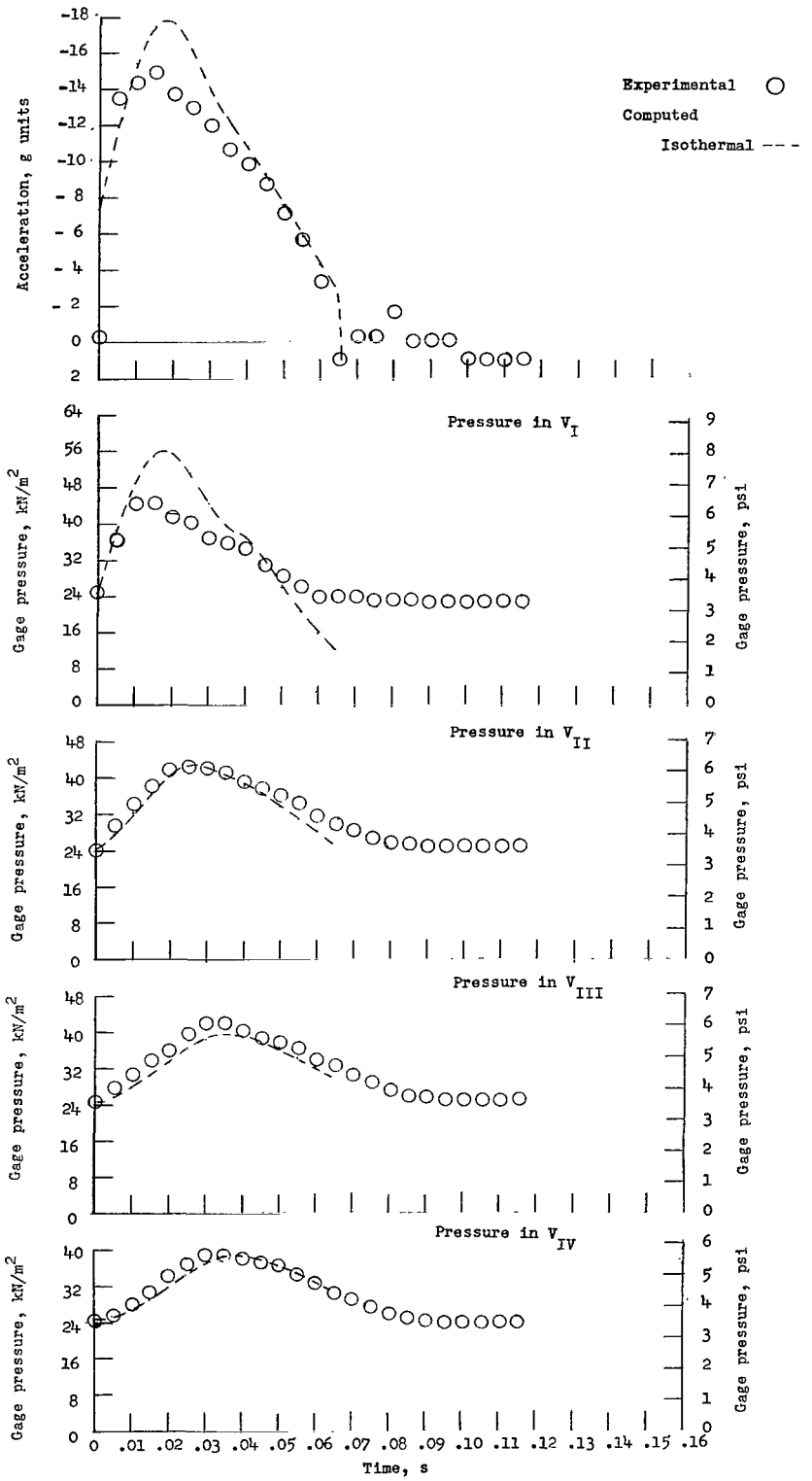

(b) Sharp-edged orifices; p_j = 24.8 kN/m^2 (3.6 psi).

Figure 6.- Continued.

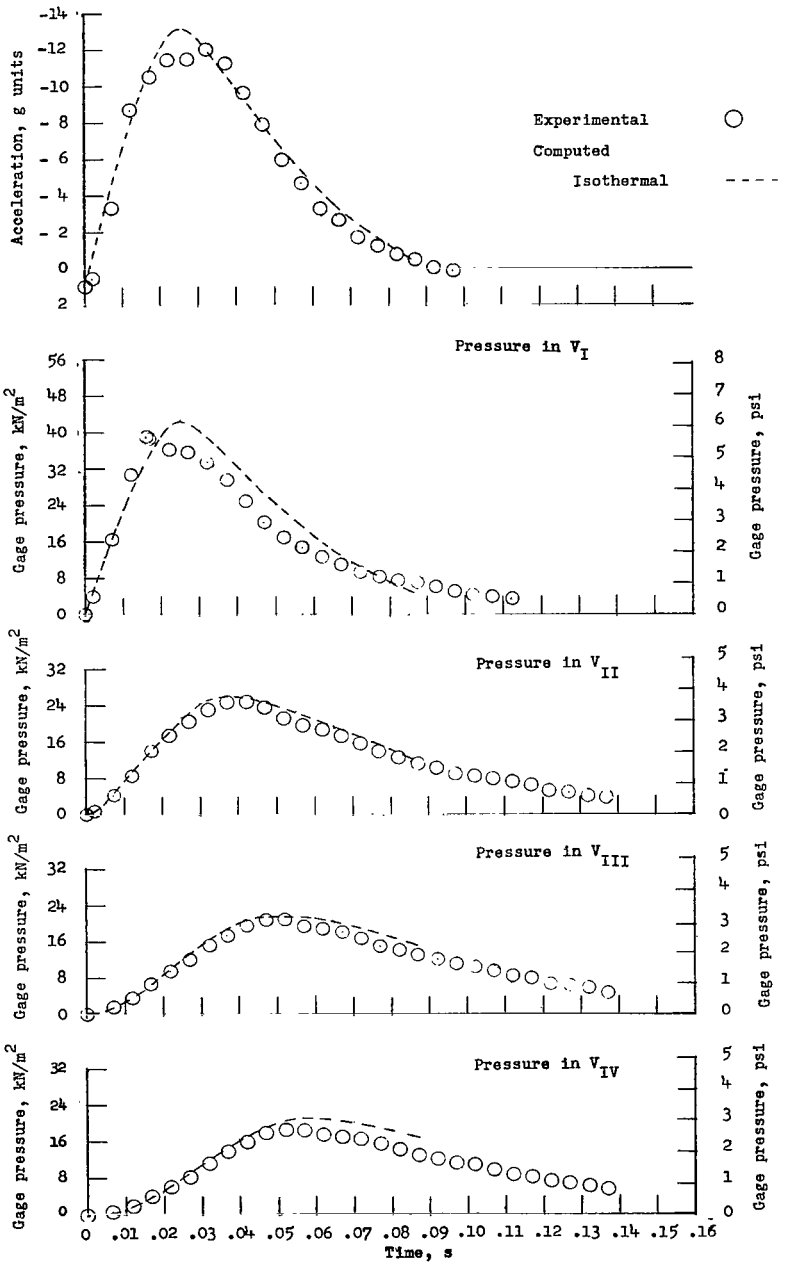

(c) Test vehicle with aircraft-fabric-covered orifices; p_i = 0 kN/m2 (0 psi).

Figure 6.- Concluded.

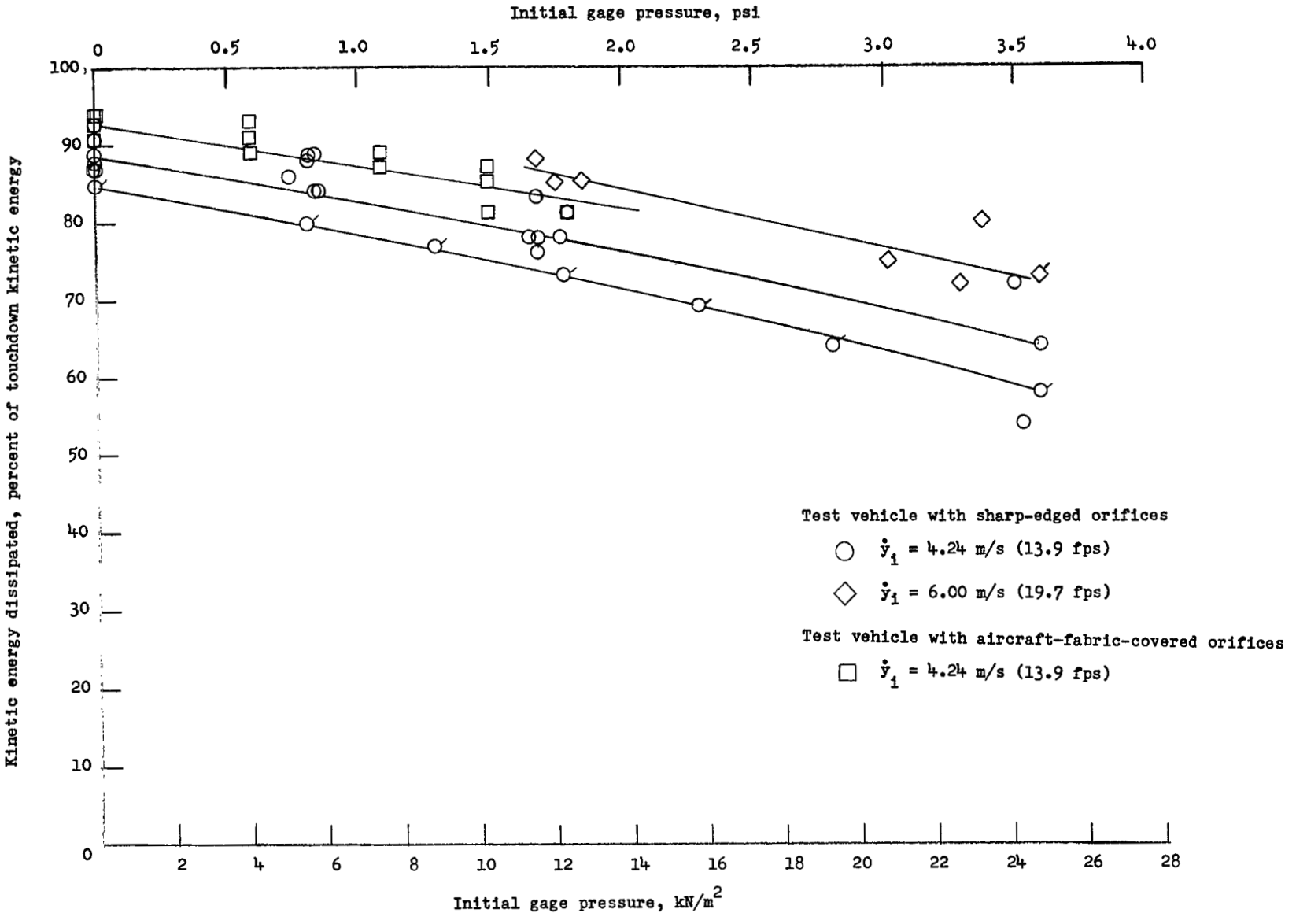

Figure 7.- Kinetic energy dissipated as a function of initial air-bag pressure. Symbols with ticks are computed data for sharp-edged orifices.

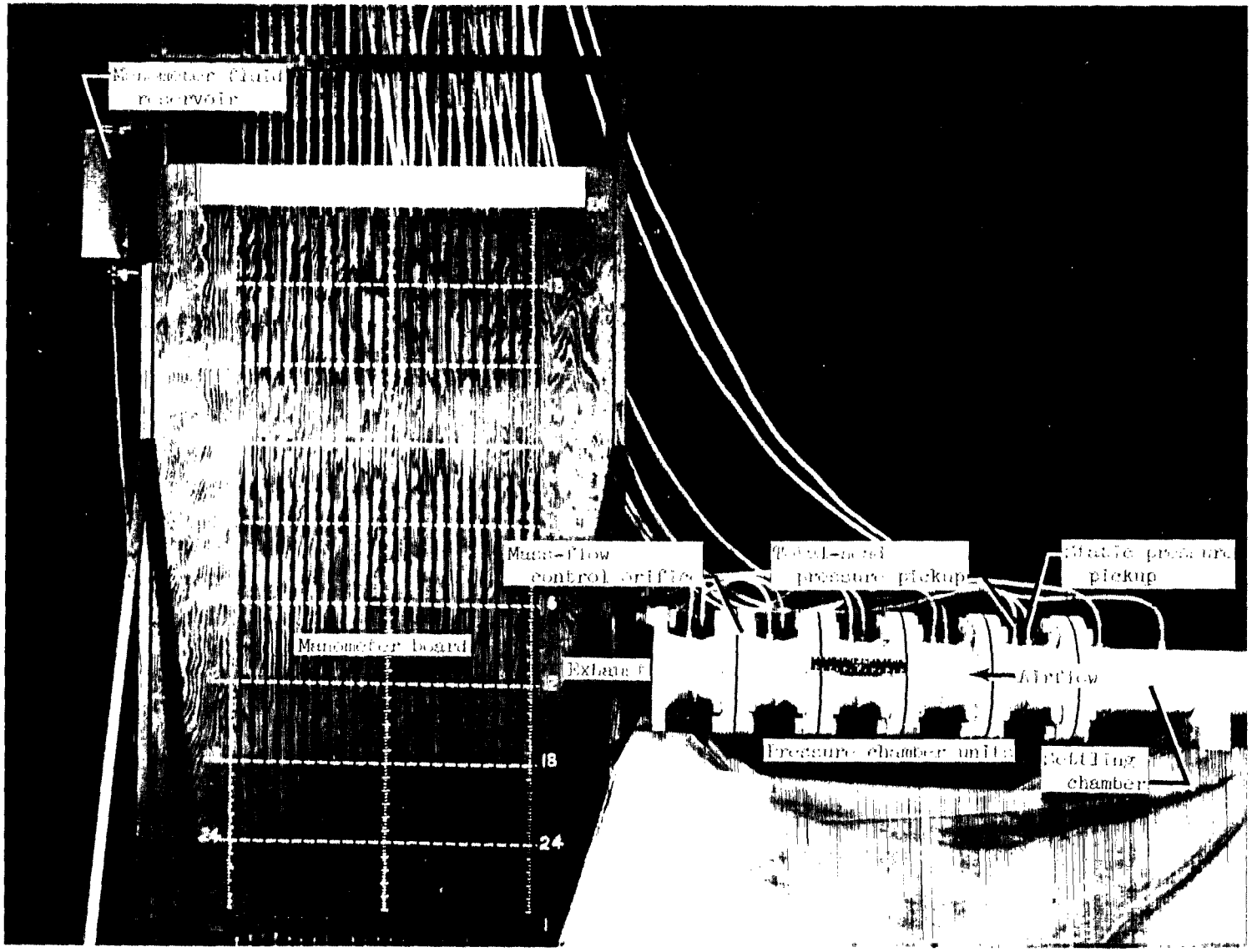

Figure 8.- Apparatus employed in discharge-parameter investigation.

L-66-3362.1

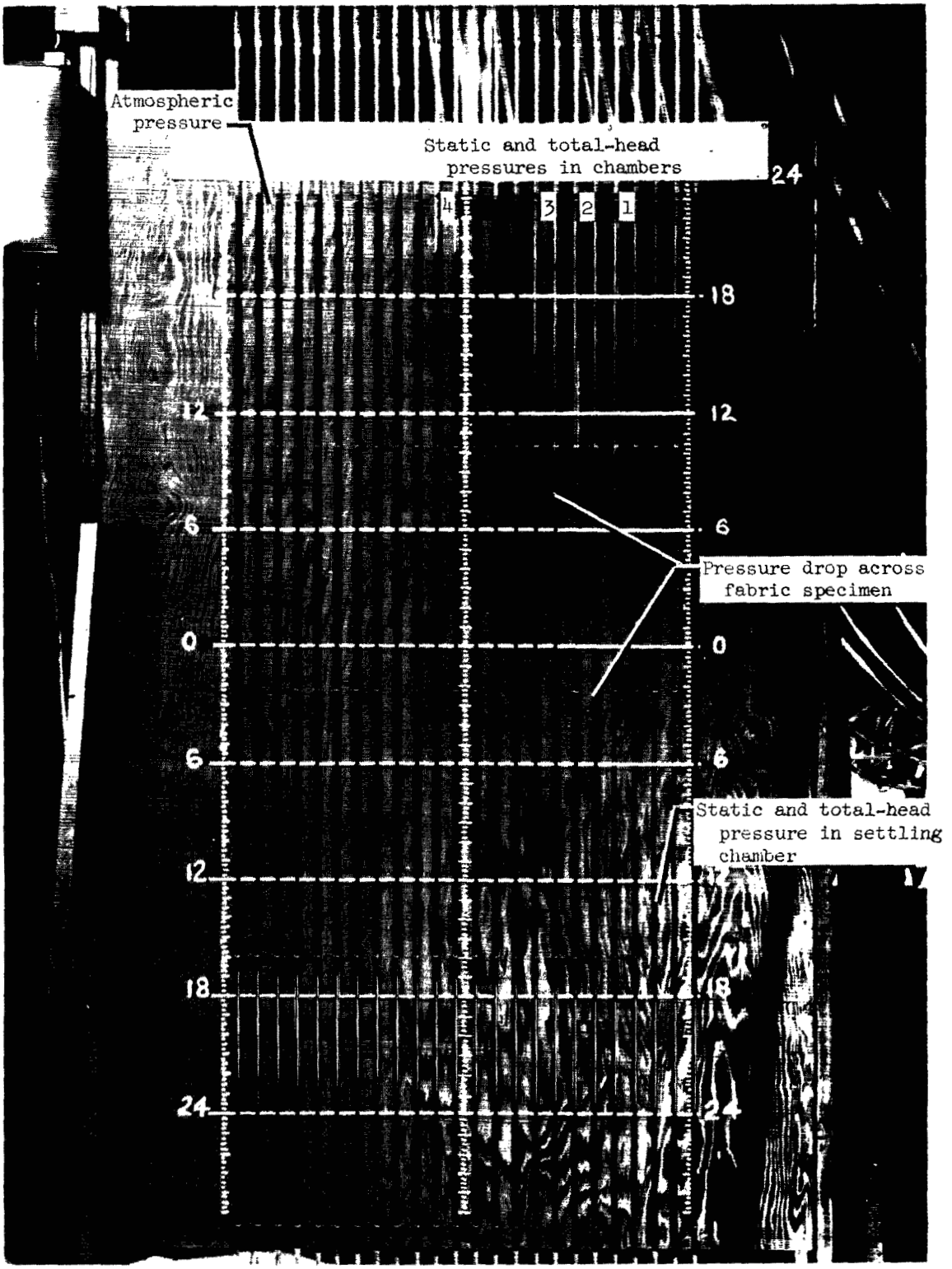

Figure 9.- Manometer board during a test.

L-66-3363.1

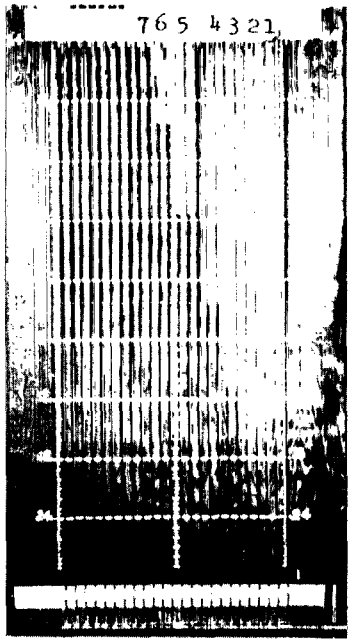

(a) Q = 0.217 g/s
(1.486 × 10^{-5} slug/sec).

Orifice	Between chambers
0.254-cm-d (0.100 in.)	1 & 2
0.254-cm-d (0.100 in.)	2 & 3
0.254-cm-d (0.100 in.)	3 & 4
0.254-cm-d (0.100 in.)	4 & 5
0.254-cm-d (0.100 in.)	5 & 6
0.254-cm-d (0.100 in.)	6 & 7

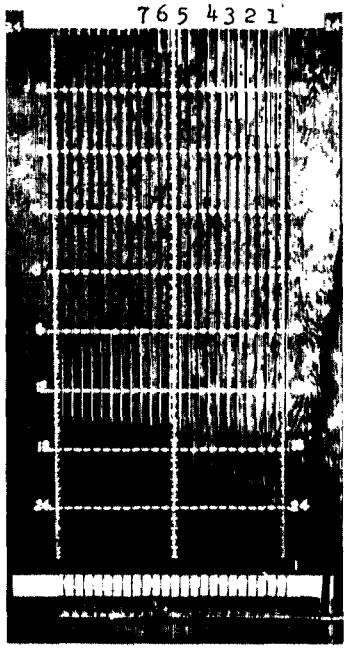

(b) Q = 8.31 g/s
(5.725 × 10^{-4} slug/sec).

Fabric or orifice	Between chambers
0.01-cm-thick (0.004 in.) type III glass	1 & 2
0.008-cm-thick (0.003 in.) type III glass	2 & 3
0.023-cm-thick (0.009 in.) type VIII glass	3 & 4
Aircraft fabric	4 & 5
Parachute fabric	5 & 6
2.357-cm-d (0.928 in.) orifice	6 & 7

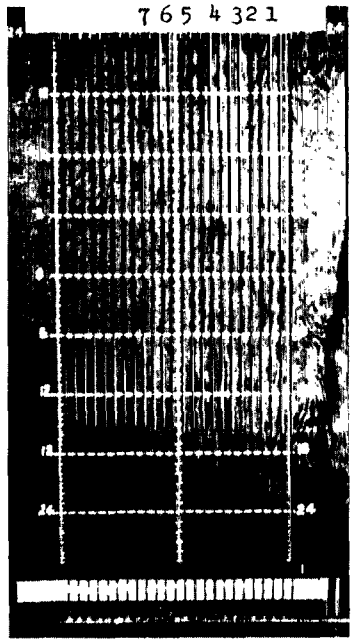

(c) Q = 8.57 g/s
(5.872 × 10^{-4} slug/sec).

Fabric or orifice	Between chambers
----------	2 removed
No orifice - no fabric	1 & 3
0.023-cm-thick (0.009 in.) type VIII glass	3 & 4
----------	5 removed
No orifice - no fabric	4 & 6
1.548-cm-d (0.609 in.) orifice	6 & 7

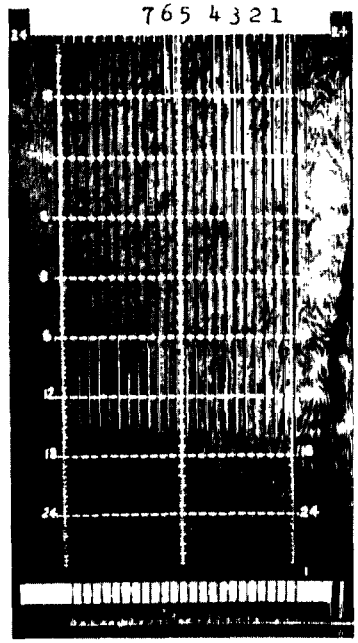

(d) Q = 7.07 g/s
(4.846 × 10^{-4} slug/sec).

Fabric or orifice	Between chambers
----------	2 removed
No orifice - no fabric	1 & 3
0.023-cm-thick (0.009 in.) type VIII glass	3 & 4
----------	5 removed
No orifice - no fabric	4 & 6
1.548-cm-d (6.09 in.) orifice	6 & 7

Figure 10.- Water-filled manometer for typical discharge parameter tests. Manometer board scales are in inches.

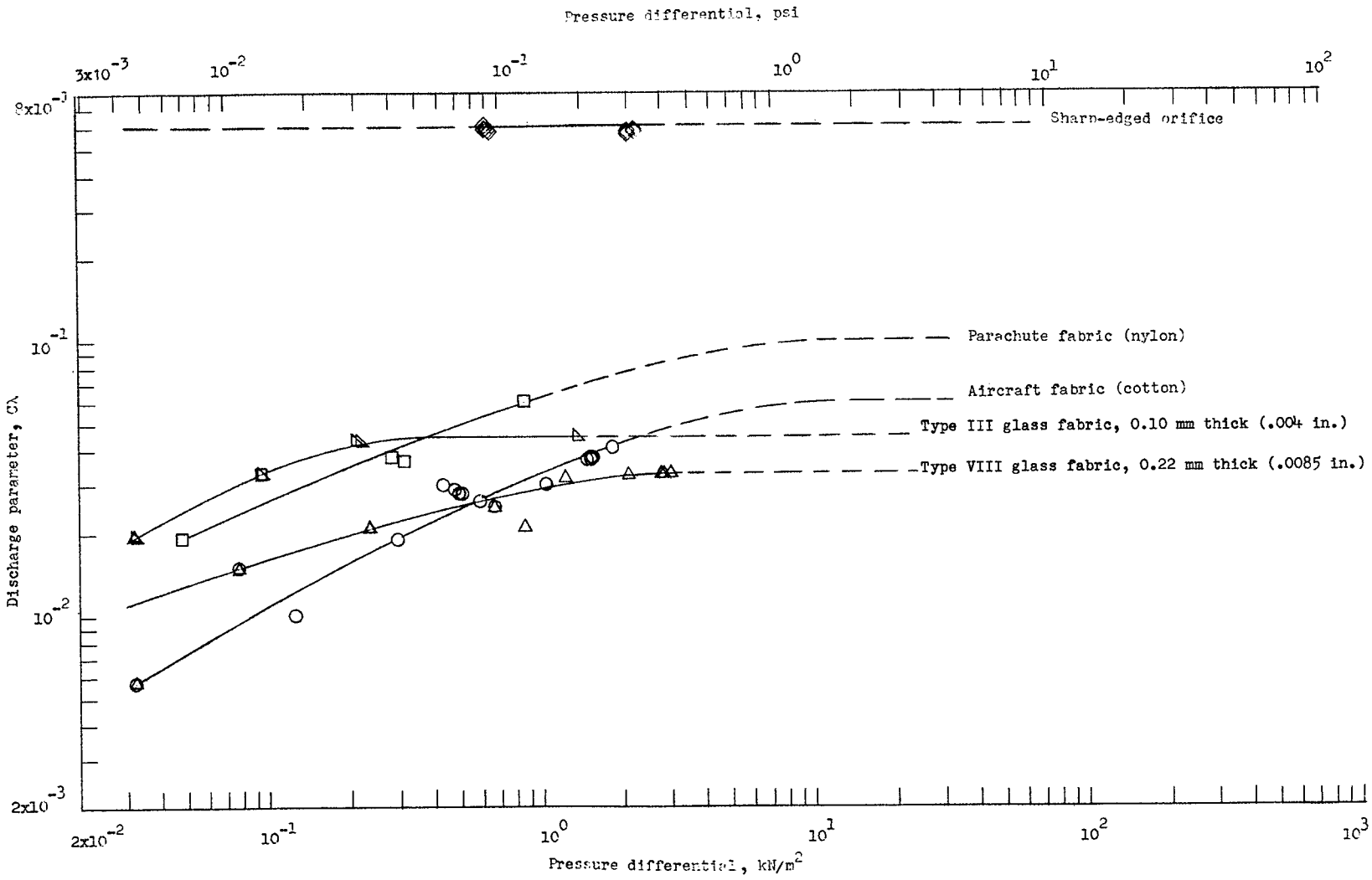

Figure 11.- Experimentally determined discharge parameters for a sharp-edged orifice and various fabrics as a function of pressure differential.

"The aeronautical and space activities of the United States shall be conducted so as to contribute . . . to the expansion of human knowledge of phenomena in the atmosphere and space. The Administration shall provide for the widest practicable and appropriate dissemination of information concerning its activities and the results thereof."

—NATIONAL AERONAUTICS AND SPACE ACT OF 1958

NASA SCIENTIFIC AND TECHNICAL PUBLICATIONS

TECHNICAL REPORTS: Scientific and technical information considered important, complete, and a lasting contribution to existing knowledge.

TECHNICAL NOTES: Information less broad in scope but nevertheless of importance as a contribution to existing knowledge.

TECHNICAL MEMORANDUMS: Information receiving limited distribution because of preliminary data, security classification, or other reasons.

CONTRACTOR REPORTS: Scientific and technical information generated under a NASA contract or grant and considered an important contribution to existing knowledge.

TECHNICAL TRANSLATIONS: Information published in a foreign language considered to merit NASA distribution in English.

SPECIAL PUBLICATIONS: Information derived from or of value to NASA activities. Publications include conference proceedings, monographs, data compilations, handbooks, sourcebooks, and special bibliographies.

TECHNOLOGY UTILIZATION PUBLICATIONS: Information on technology used by NASA that may be of particular interest in commercial and other non-aerospace applications. Publications include Tech Briefs, Technology Utilization Reports and Notes, and Technology Surveys.

Details on the availability of these publications may be obtained from:

SCIENTIFIC AND TECHNICAL INFORMATION DIVISION

NATIONAL AERONAUTICS AND SPACE ADMINISTRATION

Washington, D.C. 20546